

# **Fabrication of High Solid Silicon Microneedles Based on Anisotropic Etching by Potassium Hydroxide**

by  
Zihao Wang

A thesis  
presented to University of Waterloo  
in the fulfillment of the  
thesis requirement for the degree of  
Master of Applied Science  
in  
Electrical and Computer Engineering

Waterloo, Ontario, Canada, 2023

© Zihao Wang 2023

# **Author's Declaration**

I hereby declare that I am the sole author of this thesis. This is a true copy of the thesis, including any required final revisions, as accepted by my examiners.

I understand that my thesis may be made electronically available to the public.

# Abstract

This thesis presents the research on the high solid silicon microneedles fabrication based on KOH anisotropic etching, aiming at finding a controllable way to fabricate 500  $\mu\text{m}$  high microneedles with good height uniformity and tip sharpness. During this research, 200nm low-stress LPCVD  $\text{SiN}_x$  is used as KOH etching mask; mask shape is square-shaped with its side along  $\langle 100 \rangle$  direction of silicon wafer; wet etching is done in 29wt% KOH solution at 79°C.

In the introduction part, a general introduction of modern nanotechnology and microneedles is presented. The nanofabrication techniques that related to microneedles fabrication such as thin film deposition, photolithography, reactive ion etching, and KOH anisotropic etching are introduced for better comprehension of this research. In the experiments part, the fabrication process of microneedles is explained step by step, including  $\text{SiN}_x$  deposition and patterning, KOH wet etching, isotropic reactive ion etching using  $\text{SF}_6$ , and scanning electron microscope characterization. In the discussion part, the geometry of microneedles is studied by SEM characterization. The microneedle shape is determined as an octagonal pyramid, and its sidewall is determined as (311) plane. The aspect ratio of microneedle is 1.414. Then the growth model of microneedles in KOH etching is established. The maximum height of microneedle, obtained right after mask falling off, is positively proportional to its mask size; the real-time height of microneedle has a positive correlation during growth then, after mask falling off, a negative correlation during overetching with time. The height growth rate is 72.5  $\mu\text{m}/\text{h}$ , while the height dropping rate during over-etching is 400  $\mu\text{m}/\text{h}$ . Finally, an additional step of reactive ion

etching by using SF<sub>6</sub> gas is introduced following KOH etching before mask falling off to improve the uniformity of microneedles height, which also contributes to improve the tip sharpness. By replacing the inevitable over-etching using KOH with the SF<sub>6</sub> RIE step, the standard deviation of microneedles height decreased from 20.50 μm to 11.12 μm; the tip apex diameter decreased from 6.92 μm to 2.71 μm.

# Acknowledgements

This work was carried out in Quantum-Nano Fabrication and Characterization Facility (QNFCF) and QNC B521 laboratory at University of Waterloo. I am always grateful for the help from QNFCF staff.

I would like to thank the guidance and patience from my research group. During two years of learning and researching, my supervisor, professor Bo Cui showed excellent acknowledge in courses teaching and researches guiding, and was all the time kind, patient, and responsible to me. I also got great help and learned a lot from my group members Huseyin, Xiaoli, Aixi and Wenhan in academic study and daily life. I am sincerely appreciate their priceless care and guidance.

# Table of Contents

Author's Declaration.....	ii
Abstract.....	iii
Acknowledgements.....	v
List of Figures.....	vii
List of Tables.....	x
<b>1. Introduction.....</b>	<b>1</b>
<b>1.1 Introduction of nano/micro fabrication.....</b>	<b>1</b>
<b>1.2 Introduction of microneedles.....</b>	<b>4</b>
<b>1.3 Fabrication process of microneedles and related microfabrication Techniques.....</b>	<b>9</b>
<b>1.3.1 Thin film deposition.....</b>	<b>10</b>
<b>1.3.2 Photolithography.....</b>	<b>12</b>
<b>1.3.3 Dry etching.....</b>	<b>15</b>
<b>1.3.4 Wet etching.....</b>	<b>17</b>
<b>1.4 Formation of microneedles structures by KOH anisotropic etching.....</b>	<b>21</b>
<b>2. Experiments.....</b>	<b>26</b>
<b>2.1 SiN<sub>x</sub> thin film deposition and mask patterning.....</b>	<b>26</b>
<b>2.2 Wet etching by KOH solution.....</b>	<b>28</b>
<b>2.3 Reactive ion etching by using SF<sub>6</sub>.....</b>	<b>32</b>
<b>2.4 Characterization.....</b>	<b>33</b>
<b>3. Results &amp; Discussion.....</b>	<b>34</b>
<b>3.1 Geometry of microneedles and anisotropy of KOH wet etching.....</b>	<b>34</b>
<b>3.2 Relationship between microneedles height versus mask size and etching time.....</b>	<b>38</b>
<b>3.3 Microneedles height uniformity and tip sharpness improvement by SF<sub>6</sub> reactive ion etching.....</b>	<b>43</b>
<b>4. Conclusions.....</b>	<b>52</b>
References.....	54

# List of Figures

Figure 1.1.1 [3] Schematic diagram of (a) top-down and (b) bottom-up approach. ....	3
Figure 1.1.2 [5] Scaling of the minimum feature size patterned by each successive semiconductor technology node, compared to scaling of the source wavelength ( $\lambda$ ). ....	4
Figure 1.2.1 [7] Images of types of microneedles. Images a~d are microneedles made from silicon; Images e~h are microneedles made from metal; Images i~l are microneedles made from polymers. A and B show the under-skin drug release process of microneedles that with different release methods. ....	6
Figure 1.2.2 [8] Schematic diagram of topical cream, hypodermic needle, microneedle patch and transdermal patch. ....	7
Figure 1.2.3 [11] (a): Camera images of a mouse with the microneedle array applied. (b)(c): Wound on mice skin after microneedles patch removal. (d): Seven-day monitoring of the subcutaneous glucose levels in a normal mouse by the microneedle biosensing device (blue), in comparison with a commercial blood glucose meter for blood glucose (red). (e) Seven-day monitoring of the subcutaneous glucose levels in a diabetic mouse by the microneedle biosensing device (blue), in comparison with a commercial blood glucose meter for blood glucose. (f): Clark error grid for the microneedle biosensing device. The x-axis represents the reference blood glucose values measured by a commercial blood glucose meter, and the y-axis displays the glucose values measured by the microneedle biosensing device (the data were from eight normal and eight diabetic mice).....	8
Figure 1.3.1 Fabrication process of solid silicon microneedles. ....	10
Figure 1.3.2 [14] Overview of thin film growth on substrate surface in chemical vapor deposition.....	12
Figure 1.3.3 [16] Photolithography process with negative resist and positive resist. ....	13

Figure 1.3.4 [17] Schematic diagram of UV direct writing. ....	14
Figure 1.3.5 [18][19] Schematic diagram of Bosch process (left). Cross-section SEM image of holes done by Bosch process. ....	17
Figure 1.3.6 [20] Silicon wet etching by KOH solution. (a)schematic diagram of cross-section of (100) oriented silicon etched by KOH solution. Angle between wafer surface and sidewall is 54.7 degree. (b) SEM image of KOH etched (110) oriented silicon with line pattern. (c)SEM image of KOH etched (100) oriented silicon with square pattern. ....	18
Figure 1.3.7 [22] Etching rate and surface roughness of (100) plane versus KOH concentration at different temperature. ....	21
Figure 1.4.1 [24] Crystalline silicon atomic structure diagram. ....	22
Figure 1.4.2 [25] Microscope image of microneedle mask over increasing KOH etching time (topview). Blue area representative for the SiN <sub>x</sub> mask; Brown area representative for bare silicon. ....	24
Figure 1.4.3 SEM image of microneedles array fabricated by KOH wet etching. ....	25
Figure 2.1.1 SiN <sub>x</sub> thickness map by filmetrics. ....	27
Figure 2.1.2. Left: Layout of parts of designed masks; Colored area represent for SiN <sub>x</sub> mask. Right: SiN <sub>x</sub> mask on Si wafer; Blue area represent for SiN <sub>x</sub> mask. ....	28
Figure 2.2.1. (a) KOH etching system, including water bath equipment, beaker, and beaker cover. (b) Sample under KOH etching, with hydrogen bubbles coming out. ....	30
Figure 2.2.2 (a) Topview of microneedles with insufficient etching; (b) Topview of microneedles with sufficient etching. (c) SEM image of microneedles with reverse structure on top. ....	31
Figure 2.4.1 Phone photo of microneedles array. ....	33
Figure 3.1.1. SEM image of microneedles by KOH etching. Height of microneedle is measured as 503 μm. ....	34
Figure 3.1.2 SEM image of microneedle. Sideview of microneedle with insufficient etching from <100> direction (left). Topview of microneedle with sufficient etching (right). β <sub>1</sub> indicates the top-left angle; β <sub>2</sub> indicates the top angle. ....	37

Figure 3.2.1. (a) Layout of SiN<sub>x</sub> mask shape and size. (b) SiN<sub>x</sub> mask after reactive ion etching. Blue area indicates SiN<sub>x</sub>. (c)(d) SEM images of microneedles. Mask size of microneedles is increasing from left to right. ....39

Figure 3.2.2. Diagram of microneedles height versus original mask size with etching time 5h (blue curve), 6h (orange curve), 6.5h (gray curve). (Data from table 4) .....40

Figure 3.2.3. Diagram of microneedles height versus etching time. Black line represent the growth stage of microneedles. Colorful lines indicate the overetching stage of microneedles with variety of original mask sidelength. (Data from table 4) .....41

Figure 3.3.1. SEM image of microneedles with poor height uniformity. ....45

Figure 3.3.2. Silicon substrate phone photos after long time KOH etching. (a) Backside of substrate piece with damaged area. (b) Frontside of a half wafer, with ring structure shown under light reflection. ....45

Figure 3.3.3 SEM images of microneedles array (a) before SF<sub>6</sub> RIE, and (b) after SF<sub>6</sub> RIE. ....48

Figure 3.3.4. Diagram of height of microneedles fabricated by KOH only, and KOH + SF<sub>6</sub> etching. ....48

Figure 3.3.5 Topview SEM image of microneedle tip. (a) typical blade-shape tip with blade length=11.9 μm. (b) Sharp tip with tip diameter less than 1 μm. ....49

Figure 3.3.6. Diagram of tip diameter of microneedles fabricated by KOH only, and KOH + SF<sub>6</sub> etching. ....50

# List of Tables

Table 1. Reactive ion etching recipe for SiN <sub>x</sub> etching. ....	28
Table 2. Reactive ion etching recipe for Si isotropic etching. ....	32
Table 3. Measured and calculated etching rate of different plans and aspect ratio of microneedles. ....	37
Table 4. Microneedles height from variety of mask sizes and etching time. (microneedles with mask size less than 900um are etched over, thus data is not shown in table) ...	40
Table 5. Raw data of microneedles height and tip blade length. ....	48

# 1. Introduction

The introduction chapter briefly shows the concept and development of modern nanotechnology and nano/micro fabrication, and explain the principle of the microneedle fabrication process. Also, special techniques used in microneedle fabrication such as thin film deposition, lithography, reactive ion etching and silicon wet etching by KOH are introduced.

## 1.1 Introduction of nano/micro fabrication

On December 29, 1959, American physicist Richard Feynman gave a presentation named “There’s Plenty of Room at Bottom: An Invitation to Enter a New Field of Physics”[1], showing that properties of substance changed under 100 atoms scale, inspired the conceptual foundations of nanotechnology. 15 years later, Japanese professor Norio Taniguchi firstly used the term "nano-technology" in a conference in 1974. Techniques such as thin film deposition, ion beam milling were described as nano-technologies based on the capability of dimension control under nanometer scale. However, nanotechnology was not considered to begin developing until the invention of Scanning Tunneling Microscope in 1981. The ability of single atom scanning of Scanning Tunneling Microscope plays an important role in the rapid development of nanotechnology. In modern science, nanotechnology is described as the manipulation of matter on a near-atomic scale, typically 1~100nm, to produce new structures, materials and devices. At nanometer scale, materials begin to exhibit unique properties different from macroscopic

scale. Nowadays, nanotechnology is a highly cross-disciplinary subject that may involve theory of physics, chemistry, biology, medicine, and material science, depending on the wide applications of nanotechnology, such as Integrated Circuit (IC), Microelectromechanical System (MEMS), photovoltaic device, nanotube / nanowire, micro-optics, and so on.

Nanofabrication is the manufacture of structure and devices with at least one dimension in nanometer scale (1~100nm). “Top-down and Bottom-up” are two fundamental approaches to fabricate nanostructures. Bottom-up approach forms nano-scale structure by assembling atoms, molecular, cluster or other subunits into larger structures, with the help of chemical or physical forces such as surface tension, electrostatic force and hydrophobic-hydrophilic interactions. On the contrary, top-down approaches create nano-scale pattern on substrate materials by lithography and etching. Top-down approaches are good for producing structures with long-range order and for making macroscopic connections, while bottom-up approaches are best suited for self-assembly and establishing short-range order at nano-scale dimensions.

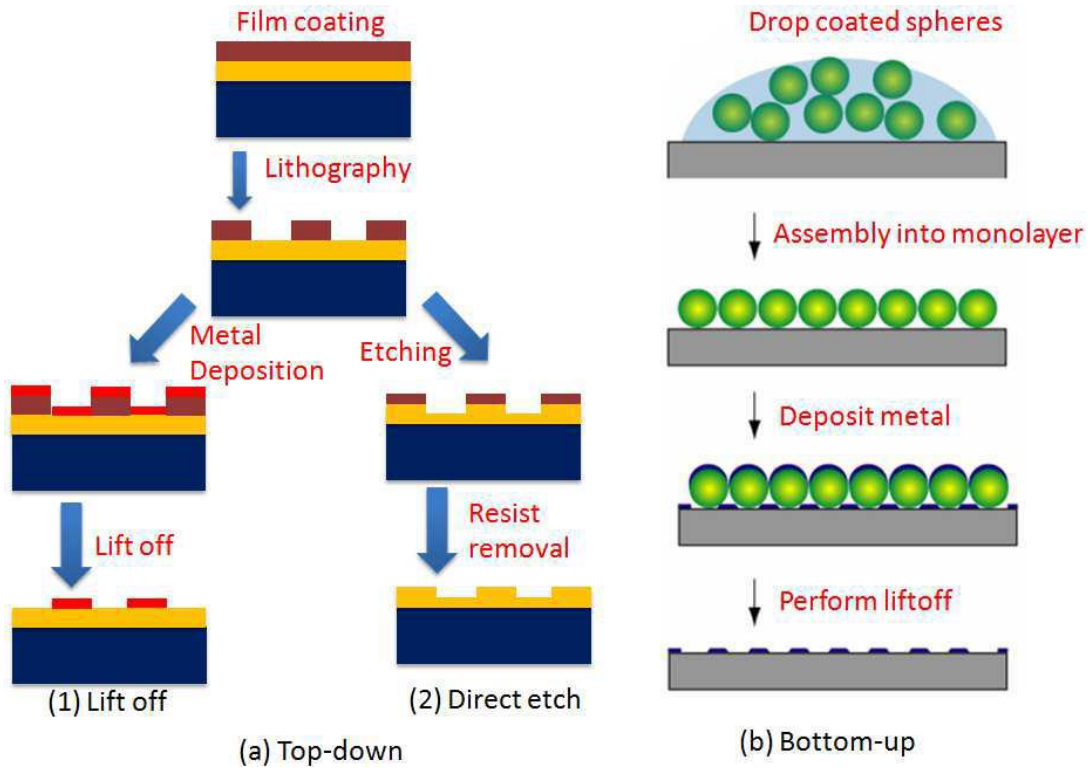


Figure 1.1.1 [3] Schematic diagram of (a) top-down and (b) bottom-up approaches.

From last decade, the demand of IC product has been dramatically increasing. Thus, a top-down strategy that involves photo lithographic patterning techniques becomes more and more popular and mature for modern IC production. By using light source with decreasing wavelength, an exponentially decreased feature size of IC product is achieved in decades. Figure 1.1.2 shows the decreasing curve of technology node and wavelength of photo lithography light source over years. The light source plays an important role in photo lithography to determine the resolution of lithography. From 1980s, the lithography light source has been developed from ultra violet (UV) generated by mercury vapor lamp (g-line=436nm, i-line=365nm) to deep UV generated by excimer laser (KrF=248nm, ArF=193nm, finally Extreme UV (EUV) generated by laser-pulsed tin plasma with wavelength of 13.5nm, which is considered the most powerful and advanced lithography

light source in IC production. The miniaturization of IC related devices dramatically reduces the size, weight, and energy consuming of electronic devices, fundamentally supports modern internet technology and big data storage and analysis.[4]

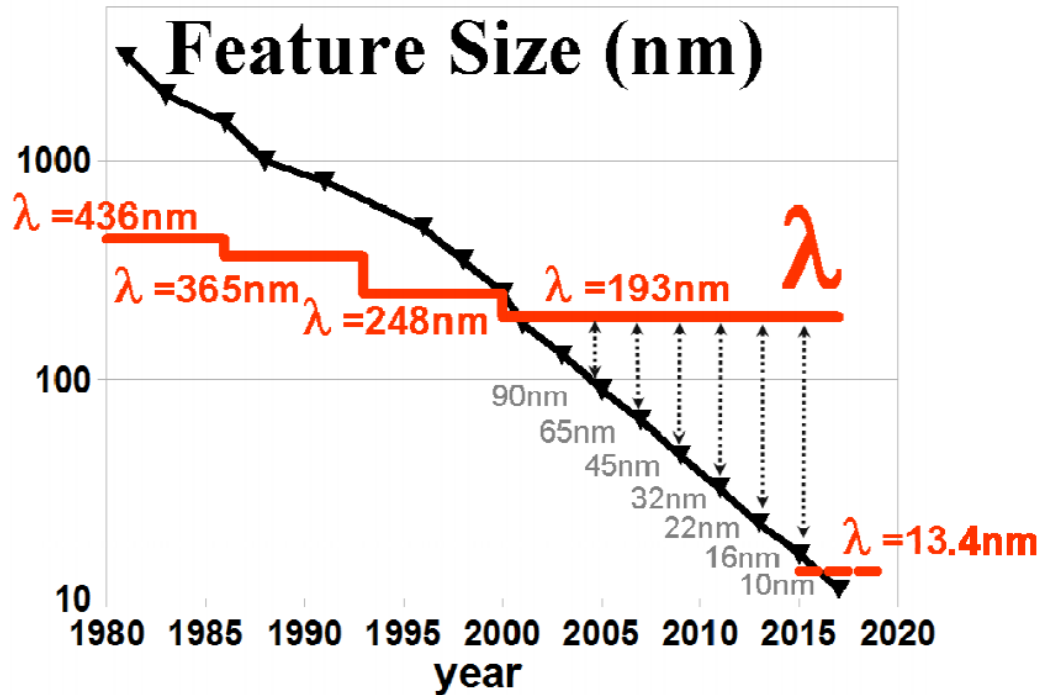


Figure 1.1.2 [5] Scaling of the minimum feature size patterned by each successive semiconductor technology node, compared to scaling of the source wavelength ( $\lambda$ ).

## 1.2 Introduction to microneedles

Microneedles are needle-shape structure fabricated by micro-nanofabrication method, typically with height from 100  $\mu\text{m}$  to 1000  $\mu\text{m}$ . Microneedles can be made from different materials and have different structures and functions depending on applications. Figure 1.2.1 shows a brief classification of microneedles. Based on the methods of functioning,

microneedles can be classified as solid microneedles, coated microneedles, dissolving microneedles, hollow microneedles and so on. In recent years, microneedle is becoming more and more popular on needles market because of its convenience and low fabrication cost and its wide applications.

During a long time in the past, oral administration of drugs was considered as the most convenient drug delivery method. However, oral administration has insolvable drawbacks when facing the challenges from the digestive tract. Drugs based on protein, DNA, and other digestible compounds that can be digested are not suitable for oral administration[6]. Moreover, oral administration takes a relatively long time to deliver drugs from mouth to blood, which may delay the treatment of drugs for time-urgent diseases. To solve the drawbacks of oral administration method, needle injection is also a popular method that can directly deliver drug into vivo. But due to the large size of the needle, disinfection process is usually needed to prevent infection on wound, and the patient also feels acute pain. Thus, there is a huge potential for microneedle patch to deliver drug by skin injection over other skin treatments. Figure 1.2.1 shows kinds of skin treatments. by adjusting the height of microneedles, penetrate epidermis can be penetrated to release drug without touching pain receptor. In recent years, applying microneedles patches on the skin becomes an attractive approach for the patients who are suffering painful injection via a hypodermic needle.

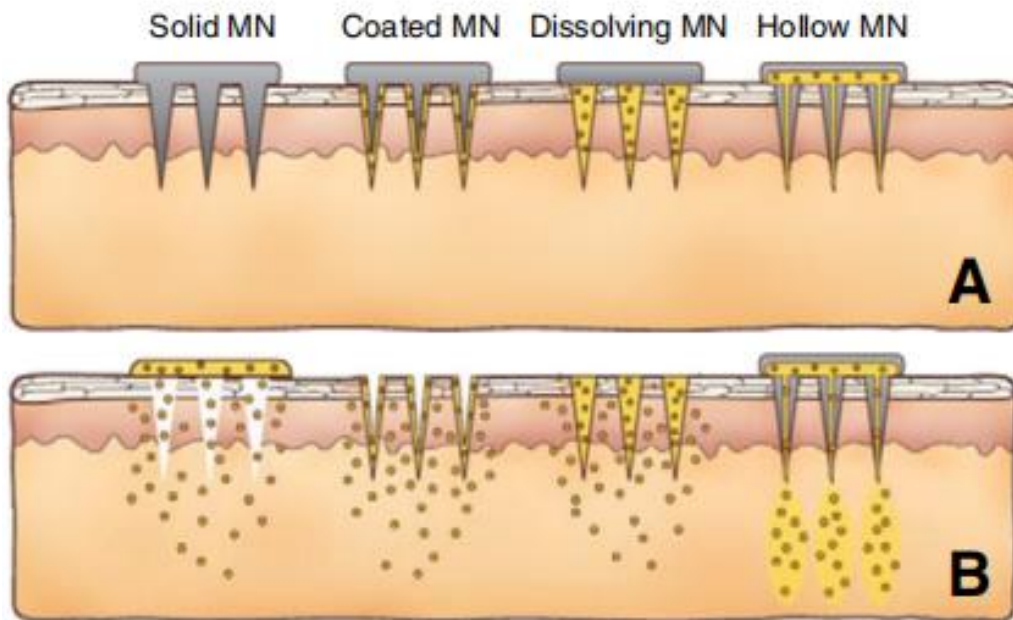
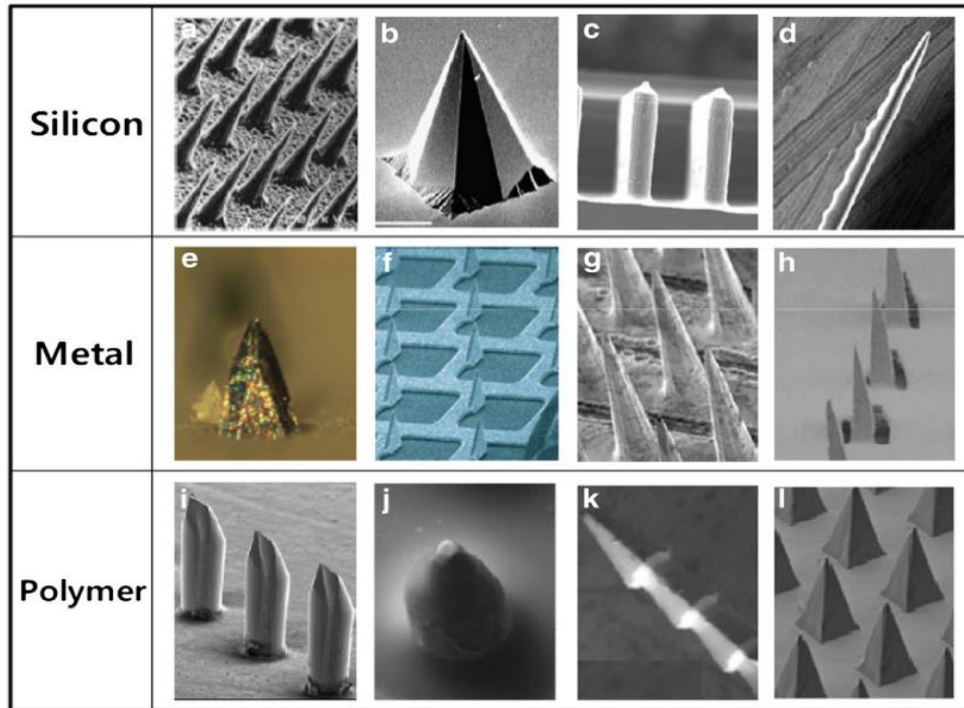


Figure 1.2.1 [7] Images of types of microneedles. Images a~d are microneedles made from silicon; Images e~h are microneedles made from metal; Images i~l are microneedles made from polymers. A and B show the under-skin drug release process of microneedles that with different release methods.

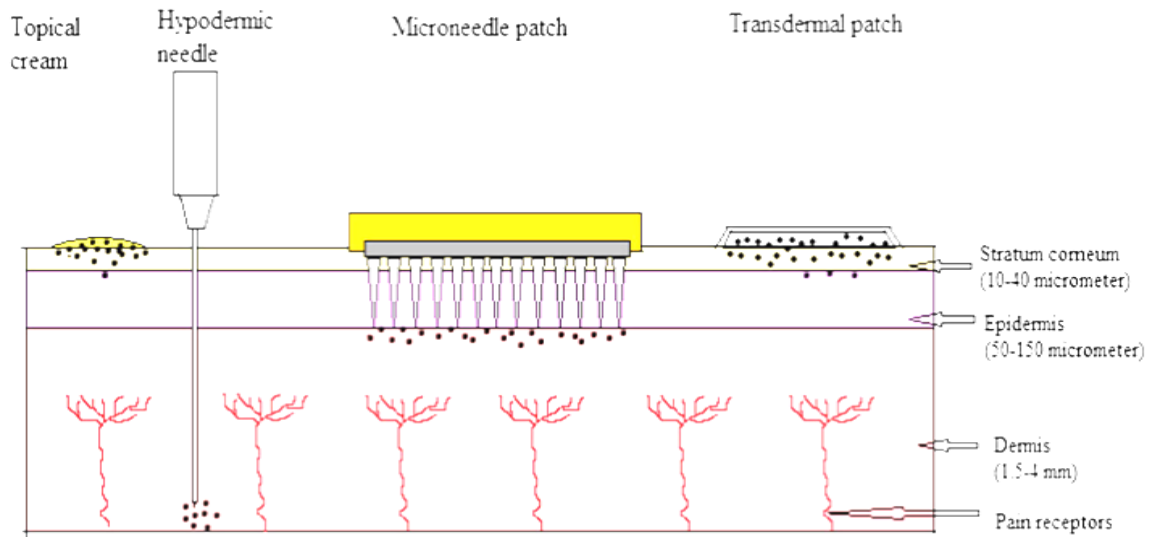


Figure 1.2.2 [8] Schematic diagram of topical cream, hypodermic needle, microneedle patch and transdermal patch.

Apart from drug delivery, microneedles also play an important role in biosensing. The high aspect ratio structure allows microneedles function as a sensor or sensor carrier to achieve sensing in vivo such as glucose, DNA and proteins. One of the most popular applications of microneedles in biosensing is blood glucose monitoring. Diabetes is one of the most prevalent and challenging diseases of the 21st century. Currently, approximately 10% of the world's population has diabetes, and approximately 1.5 million people die directly from diabetes yearly.[9][10] The monitoring of blood glucose and medicine administration is necessary for diabetes patients to control the blood glucose level. However, the traditional fingerstick glucose test using commercial glucose meters could cause pain to patients, accompanied by possible infections and complications. Moreover, it can only provide one glucose level at one time, which has low efficiency in blood glucose management. Microneedles as sensing device have several advantages compared to

traditional fingerstick glucose test. Firstly, by applying a microneedles patch on skin, the blood glucose level can be monitored continuously, achieving a more accurate blood glucose management. Secondly, microneedles patch creates smaller wounds and less pain than fingerstick test, achieving a more comfortable blood glucose management for diabetes patients. Figure 1.2.3 shows *in vivo* monitoring of subcutaneous glucose in mice with the microneedles patch biosensing device, compared with biosensing by commercial blood glucose meter.

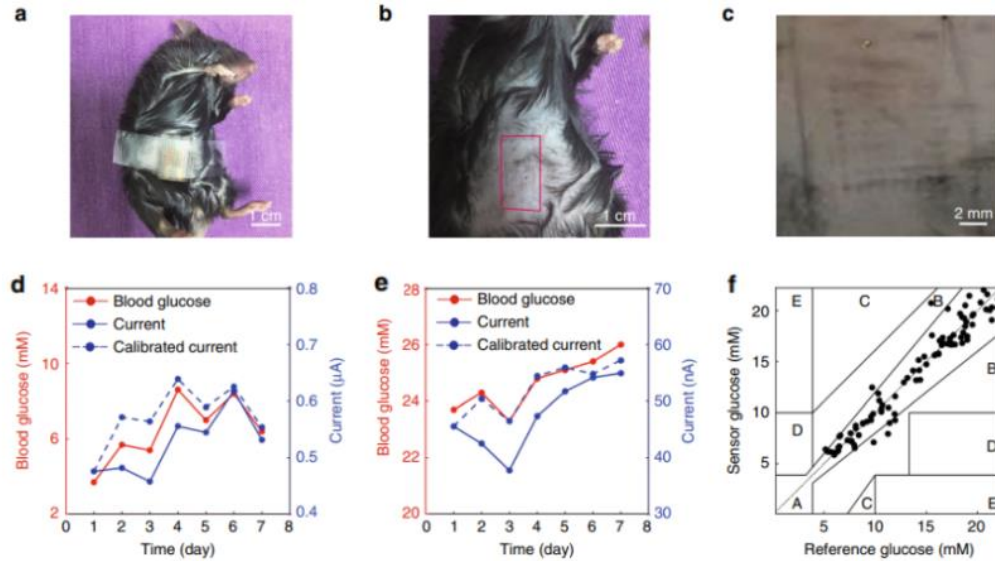


Figure 1.2.3 [11] (a): Camera images of a mouse with the microneedle array applied. (b)(c): Wound on mice skin after microneedles patch removal. (d): Seven-day monitoring of the subcutaneous glucose levels in a normal mouse by the microneedle biosensing device (blue), in comparison with a commercial blood glucose meter for blood glucose (red). (e) Seven-day monitoring of the subcutaneous glucose levels in a diabetic mouse by the microneedle biosensing device (blue), in comparison with a commercial blood glucose meter for blood glucose. (f): Clark error grid for the microneedle biosensing device. The x-axis represents the reference blood glucose values measured by a commercial blood glucose meter, and the y-axis displays the glucose values measured by the microneedle biosensing device (the data were from eight normal and eight diabetic mice)

### **1.3 Fabrication process of microneedles and related microfabrication techniques**

Solid silicon microneedles can be fabricated by following a standard microfabrication process including low pressure chemical vapor deposition (LPCVD), spin coating of resist, UV lithography, reactive ion etching (RIE), silicon wet etching by KOH, and characterization by scanning electron microscopy (SEM). Figure 1.3.1 shows a brief solid silicon microneedles fabrication process flow by N. Wilke [12]. Silicon wafer with (100) orientation is chosen as substrate to achieve specific anisotropy. Thin film of  $\text{SiO}_2$  and  $\text{SiN}_x$  is deposited on both sides of silicon wafer by low pressure chemical vapor deposition (LPCVD). Then by photo lithography and plasma etching, the designed mask shape is patterned on  $\text{SiN}_x$  film. By using  $\text{SiN}_x$  as wet etching mask, sample is immersed into KOH solution at 79 degree Celsius. KOH solution is used as etchant of silicon. As the etching goes on, due to the undercut created by silicon etching, mask will shrink and finally falls down. The wet etching is considered finished when mask falls down and microneedle structure is obtained.

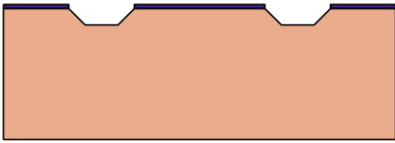
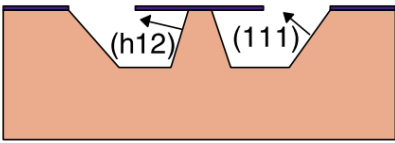
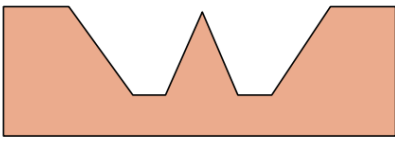
	Side View	Process step
1		LPCVD, 350Å pad oxide and 1000Å nitride double layer on silicon
2		Plasma etch to pattern mask
3		Wet etch using 29% KOH @ 79°C, etch of (111) crystal planes
4		High index crystal plane formation
5		Process stop

Figure 1.3.1 Fabrication process of solid silicon microneedles.

### 1.3.1 Thin film deposition

In most cases, thin film deposition is the first step during microfabrication process to create device with semiconductor materials or stop layer such as SiO<sub>2</sub>. There is plenty of

methods that can be chosen to achieve specific applications [13]. Thin film deposition can be divided into chemical vapor deposition (CVD) such as low pressure chemical vapor deposition (LPCVD), plasma enhanced chemical vapor deposition (PECVD), atomic layer deposition (ALD), and physical vapor deposition (PVD) such as thermal evaporation and sputtering. Each technique has its own advantages depending on materials, target thickness, and desired properties of thin film. Typically, chemical vapor deposition is used for non-metal material deposition such as  $\text{SiO}_2$ ,  $\text{SiN}_x$ . While physical vapor deposition is usually used for metal or metal oxide material such as aluminum, chromium, copper and their oxides. Importantly, one material deposited by different techniques may result in different properties and quality. Figure 1.3.2 shows the steps of thin film growth in a chemical vapor deposition process. First the substrate is exposed to volatile precursors which are formed from supplied gases. Then the reaction on the substrate surface produces the desired deposition. Normally CVD contains various physical and chemical processes which involves complex fluid dynamics since gases flow into the reactor and participate complex reactions, and also by-products are mean to be transported out of the reactor.

For  $\text{SiN}_x$  deposition in this thesis, LPCVD is a prior choice against PECVD, since LPCVD  $\text{SiN}_x$  has a much higher etching resistance (1~2nm/hr) than PECVD  $\text{SiN}_x$  (200~300nm/hr) against KOH etching. Thus,  $\text{SiN}_x$  film in this thesis is done by LPCVD to achieve long time KOH etching.

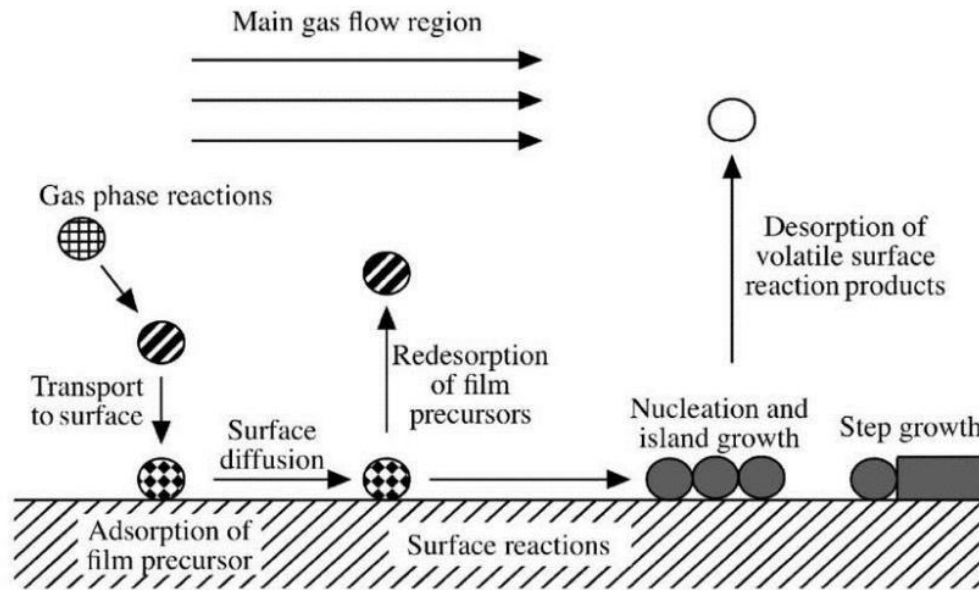


Figure 1.3.2 [14] Overview of thin film growth on substrate surface in chemical vapor deposition.

### 1.3.2 Photolithography

Developed in 1959, photolithography is a process that allows high-intensity light and a photomask to produce a polymer pattern on substrate[15]. The polymer coated on substrate, which is usually photoresist, will show a different solubility in developer at exposed area and non-exposed area. As a result, pattern is achieved by partial dissolving of resist. Positive resist and negative resist are two type of resists that have opposite property against light exposure. Figure 1.3.3 shows the lithography process of positive resist and negative resist. Positive resist has a higher solubility after exposure. As a result, area with sufficient exposure will show no positive resist after development. On the contrary, negative resists will cross-link during exposure, thus well exposed area will show negative resist remaining.

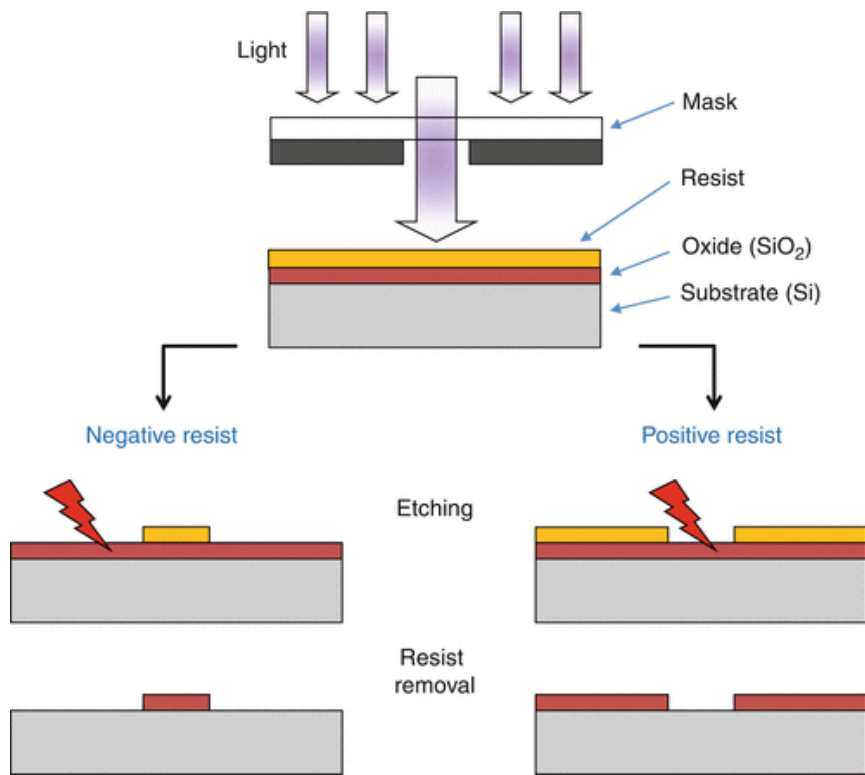


Figure 1.3.3 [16] Photolithography process with negative resist and positive resist.

Photolithography can be considered as the key technique in modern semiconductor industry since nano-scale structure can be patterned by this technique. Since photolithography was developed, people never stop improving its resolution to minimize the size of semiconductor device. Though deep UV lithography and extreme UV lithography are most commonly used in chips production, other kinds of lithography such as X-ray lithography, electron-beam lithography, focused ion beam lithography, and nano-imprint lithography also play important roles and have their own suitable applications.

As a purpose of patterning microneedles mask, maskless aligner (MLA) using 375nm or 405nm light source is a good choice since no photomask is needed, which dramatically

reduce the time and cost of mask design and fabrication. By controlling an array of reflecting mirrors, a frame can be directly patterned by partial light exposure. In order to enlarge pattern area, stage can move frame by frame following the direction of stripe. Then larger area is exposed stripe by stripe. Thus, for single substrate exposure, MLA takes longer time than mask aligner. However, be free of photomask can save much more time and money even with longer exposure time since mask design changes all the time in scientific research. Typically, UV lithography can achieve a resolution under  $1\ \mu\text{m}$ , which is completely sufficient compared to the size of microneedle mask which is more than  $10\ \mu\text{m}$ .

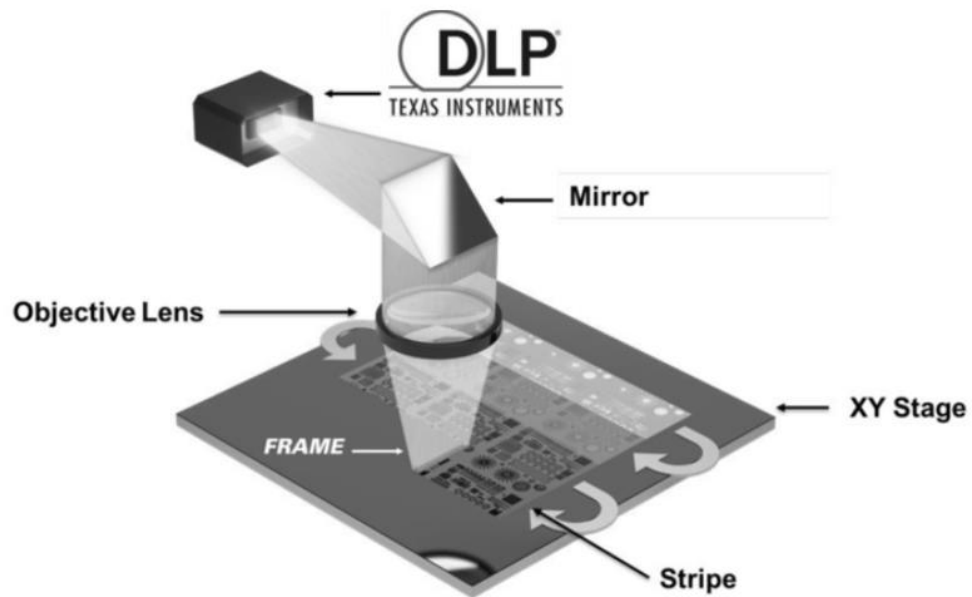


Figure 1.3.4 [17] Schematic diagram of UV direct writing.

### 1.3.3 Dry etching

When resist or soft mask is patterned, etching is introduced to transfer pattern to substrate. In order to achieve good etching result, the selectivity between substrate material and mask should be high enough to allow mask to protect underneath material from etching. Thus etching-resisted materials are chosen as mask in different etching methods and conditions. Generally, two types of etching are widely used in micro-nanofabrication, which are called dry etching and wet etching classified by the reaction environment.

Reactive ion etching (RIE) is the most commonly used dry etching method. A wide range of materials such as silicon, silicon compounds, and metals can be etched by RIE with variety of etchant gases. Usually photoresist and metal or metal oxide are widely used as mask materials in reactive ion etching since they have strong resistance against specific ion etchant. There are several important metrics that may need to be controlled in the etching process such as uniformity among the wafer, etch rate, selectivity between substrate material and mask material, anisotropy, undercut and profile, and so on.

Bosch process is a commonly used process in reactive ion etching of silicon. Bosch process is named after the German company Robert Bosch GmbH which patented the process. It is a repeating process with etching step and deposition step alternating. In Bosch process, the first etching step is an isotropic etching step which uses radical from  $\text{SF}_6$  plasma, normally obtain an etching depth of 0.5  $\mu\text{m}$  to 1  $\mu\text{m}$ . Then deposition step and etching step are proceeded alternately to form a nearly vertical profile. Deposition step generates a passivation layer of fluorocarbon on silicon surface by  $\text{C}_4\text{F}_8$  plasma. The passivation layer is composed of chains of a Teflon-like polymer that will not react with the etch plasma. So that covered silicon can be protected from further etching. Then an etching step is following, which is actually two steps of etching. In first etching step, a bias

is applied to accelerate the reactive ion to physically and directionally sputter away the polymer on bottom surface, while the passivation layer at sidewall is remaining. Then the main silicon etching step is processed with  $\text{SF}_6$  gas to isotropically etch silicon. By switching the recipe between etching and deposition in cycles, anisotropy is maintained on final structure. Moreover, by accumulating the vertical etching, a high aspect ratio can also be obtained in Bosch process easily. However, anisotropic etching in Bosch process is achieved by stack of  $\text{SF}_6$  isotropic etching steps, which causes the profile showing scallop-like shape, leading to an obvious roughness of the sidewall. Figure 1.3.5 shows a schematic diagram of Bosch process and the SEM image of holes etched by Bosch method. As a key method in DRIE, Bosch process is widely used in fabrication of DRAM, MEMS, electronics, and so on. Today, the Bosch process still stands out in many applications from other anisotropic etching methods such as cryogenic etching and wet etching.

In this thesis, reactive ion etching is used to pattern the  $\text{SiN}_x$  mask and etch the microneedles.  $\text{CHF}_3$  and  $\text{O}_2$  gas is used for  $\text{SiN}_x$  mask patterning; And  $\text{SF}_6$  gas is used at final stage etching for microneedles.

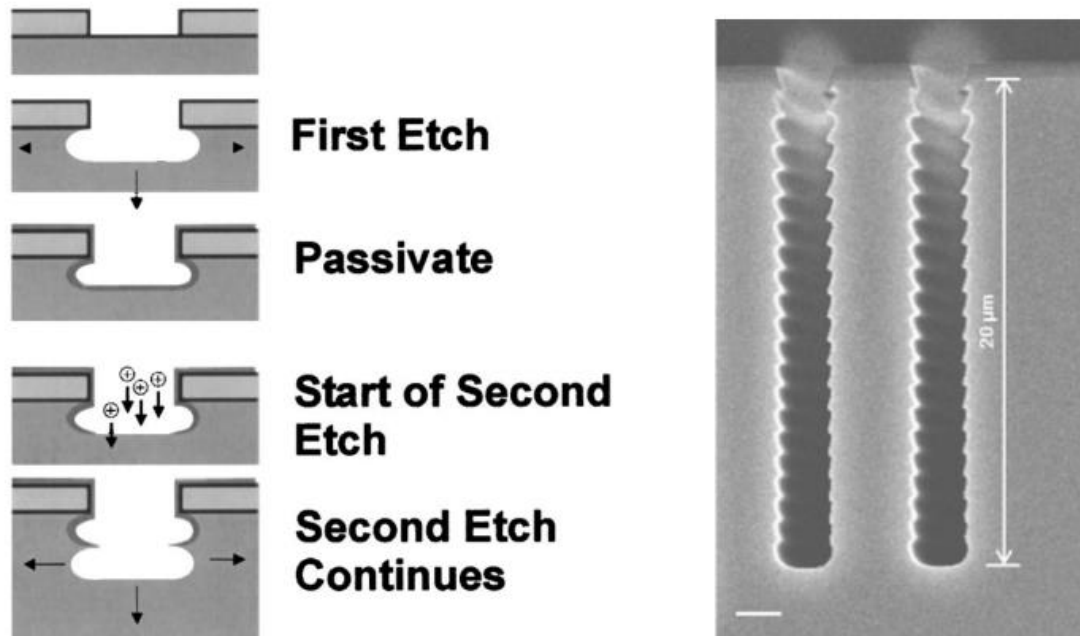


Figure 1.3.5 [18][19] Schematic diagram of Bosch process (left). Cross-section SEM image of holes done by Bosch process.

### 1.3.4 Wet etching

Apart from dry etching, wet etching is also a widely used etching methods in micro-nano fabrication. Referring to its name, wet etching is the etching process of solid materials in a chemical solution. Comparing to dry etching, wet etching is more efficient for etching silicon, oxide, and metals with a relatively large area, and easier to proceed due to less critical requirements such as energy, vacuum, temperature. Silicon wet anisotropic etching is extensively used in silicon bulk micro-machining for the fabrication of Microelectromechanical Systems (MEMS) and surface texturing for solar cell applications. Similar to dry etching, different wet etching methods can result in either isotropic etching or anisotropic etching.

Potassium hydroxide (KOH) solution and tetramethylammonium hydroxide (TMAH) are commonly used as etchants for silicon anisotropic etching. Different from Bosch process, the anisotropy is obtained by the large etching rate difference between different crystalline planes in single crystal silicon. Figure 1.3.6 shows the profile in anisotropic wet etching by using KOH solution.

Etching of silicon wafer with (100) orientation results in a pyramid-shaped pit. (111) planes are shown as sidewalls since (111) planes have the lowest etching rate. The angle is 54.7 degree between (111) plane and (100) plane; 90 degree between (110) plane and (100) plane.

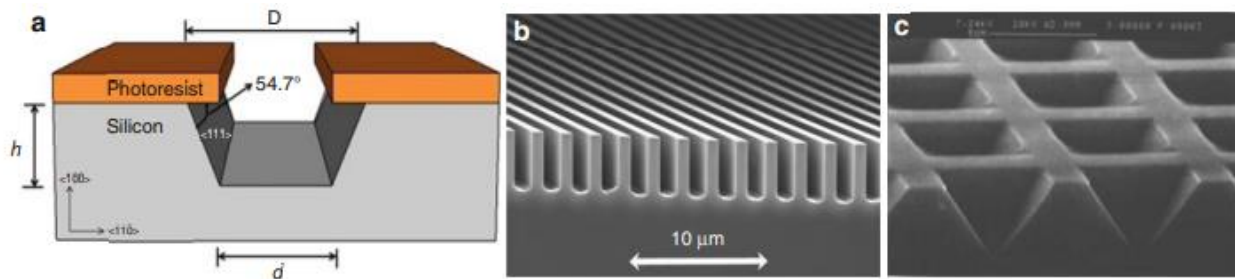
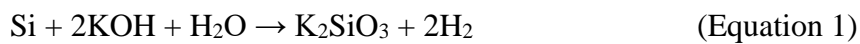
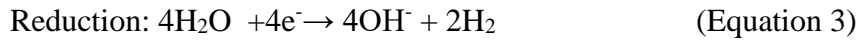
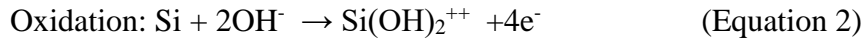


Figure 1.3.6 [20] Silicon wet etching by KOH solution. (a) schematic diagram of cross-section of (100) oriented silicon etched by KOH solution. Angle between wafer surface and sidewall is 54.7 degree. (b) SEM image of KOH etched (110) oriented silicon with line pattern. (c) SEM image of KOH etched (100) oriented silicon with square pattern.

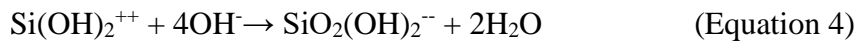
Normally several chemical reactions get involved in a single wet etching process. As an example for KOH etching, the overall chemical reaction is



Which can be decomposed into a reduction reaction, an oxidation reaction, and a following neutralization reaction:



Silicate further reacts with hydroxyl group to form a water soluble complex:



From equation 1, it is known that Si is oxidized into solution and Hydrogen is reduced to gas and emit from solution. However, overall reaction is not enough to understand the complex reactions happening in etching and shows nothing related to reaction mechanism. By decomposing overall reaction into partial equations, etching mechanism can be revealed and factors related to etching rate such as KOH concentration and temperature can be studied to get a better control of etching process. A general relationship between the silicon etch rate and surface roughness versus KOH concentration and temperature is shown in figure 1.3.7. The etch rate increases with temperature; while decreases with KOH concentration for not too low (below 10%) concentration, which is kind of opposite to common sense because here water is a reactant rather than a diluent. Many researchers have launched researches on the effects of KOH concentration on silicon etching rate, and have drawn a general conclusion that the etching rate decreases with increasing KOH concentration [21]. This phenomenon can be explained by equation 2 and equation 3 that

show water as the actual etchant of silicon. As the concentration of KOH increases, the concentration of water decreases and leads to a decreasing of etching rate. Moreover, since the etching rate depends on the partial reaction with the lowest rate that is the reduction of hydrogen, hydroxyl group from KOH is considered excessive. As a consequence, high concentration KOH has a negative effect on etch rate. However, on the other hand,  $\text{Si(OH)}_2^{++}$  formed in the redox reaction is unsolvable, which covers the silicon surface as passivation layer to stop further etching. Hydroxyl group from KOH participates the following neutralization reaction to dissolve the passivation layer silicate to solvable complex (equation 4). Thus not the concentration but the presence of alkaline solution plays a necessary role in silicon etching.

Figure 1.3.7 also shows the surface roughness is decreased to less than 100nm when the concentration of KOH is above 27%. As a consequence, 29% is the point that both have acceptable etching rate and good surface roughness. In this thesis, the etching solution is chosen as 29% KOH solution at 79 degree. Temperature above 100 degree will not be used since water bath cannot reach 100 degree.

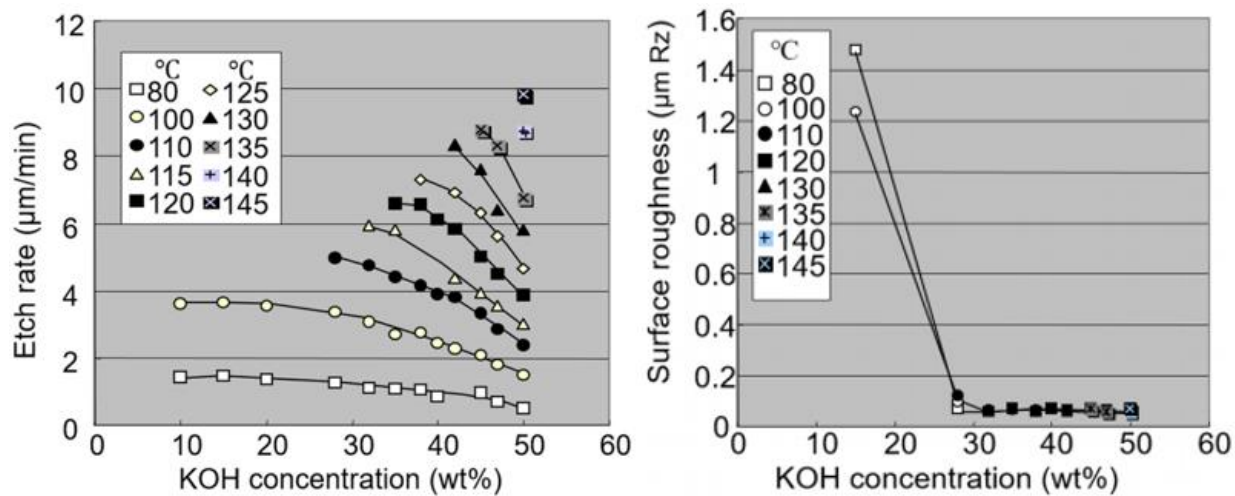


Figure 1.3.7 [22] Etching rate and surface roughness of (100) plane versus KOH concentration at different temperature.

#### 1.4 Formation of microneedle structures by KOH anisotropic etching

As mentioned, anisotropic etching of crystalline silicon can be obtained by using Alkaline solution such as KOH, and the anisotropy is achieved by large etch rate difference of different crystalline planes. The etch rate of different planes depends on the density of atoms in plane, and the energy of frontside dangling bonds and backside Si-Si bonds. Figure 1.4.1 shows a clear illustration of surface atoms and bonds at different planes. As for bond number, one silicon atom has 1 dangling bond and 3 back Si-Si bonds in (111) plane; 1 dangling bond, 2 surface Si-Si bonds and 1 back Si-Si bond in (110) plane; 2 dangling bonds and 2 back Si-Si bonds in (100) plane and high index planes such as (311) and (331) plane. The more dangling bonds and less back side Si-Si bonds an atom has, the easier for etching the atom. Thus, in most cases, (111) plane with only one dangling bond and 3 Si-Si bonds has the lowest etch rate against KOH solution; while planes with two or

more dangling bonds have higher etching rate. Besides, high index planes have a higher etching rate than (100) plane because the asymmetric bond structure leads to a lower energy in Si-Si bonds. Last but not least, (110) plane always has a higher etch rate than (100) plane (unless if surfactant such as IPA is added). One convincing explanation is that (110) plane fits the direction of atomic channel, which allows etchant to achieve a better penetration into silicon [23].

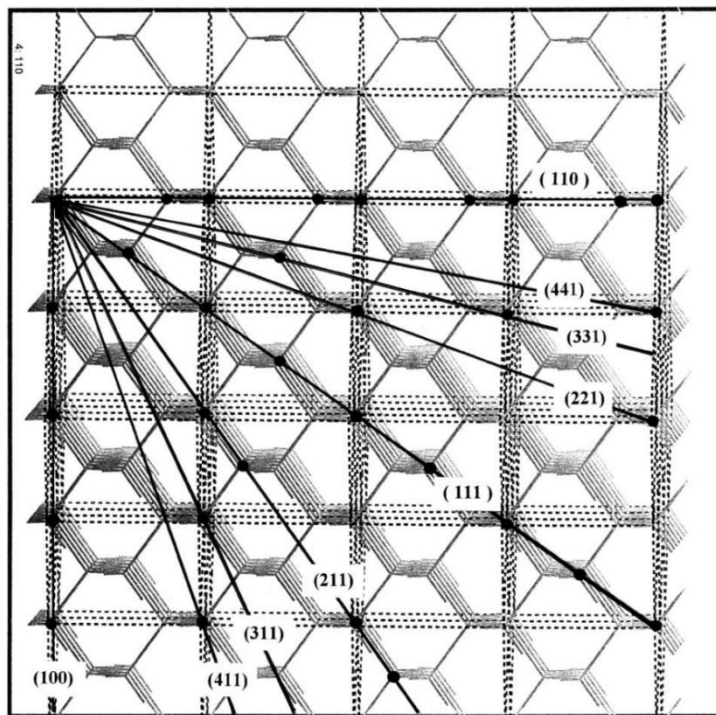


Figure 1.4.1 [24] Crystalline silicon atomic structure diagram.

Different from the trench etched by KOH with (111) plane as sidewall, microneedles shape is formed starting with convex corners on  $\text{SiN}_x$  mask. Convex corner is the corner of the mask that is less than 180 degree, which means that the mask pattern on wafer is

isolated by continuous silicon. For example, square or triangle shaped mask are convex cornered structures that lead to a final microneedle structure. On the contrary, mask with concave corners will end up as trench with (111) plane as sidewall. Figure 1.4.2 shows the formation of microneedles, which is composed of 3 stages etching:

1. At the beginning, (111) plane is shown as sidewall since it has the lowest etch rate. At the same time, high index plane is formed at convex corner, and gradually take over (111) as new sidewall due to higher etch rate. (Shown in figure 1.4.2, 0-150min)

2. When high index plane completely takes over (111), an octagon is formed and can be observed from top view. Then eight sidewalls begin to shrink toward center until mask falls down. Final microneedles structure is formed. (Shown in figure 4, 150min- 350min)

3. After mask falls down, the silicon microneedle is further etched. The overetching causes a fast drop of microneedles' height. However, the microneedles still keep the original structure regardless of the size shrinkage. At the end of the overetching, microneedles disappear and bare (100) surface is left. Figure 1.4.3 shows the SEM image of microneedles fabricated by KOH etching.

In summary, the introduction section briefly presents the concept and development of micro-nanofabrication and the fabrication methods of microneedles. In order to enhance the understanding of the whole fabrication process, techniques related to or used in microneedles fabrication are introduced such as thin film deposition, lithography, reactive ion etching, KOH wet etching. Moreover, the mechanism of formation of microneedles during KOH etching is equally important for carrying out researches on microneedles fabrication.

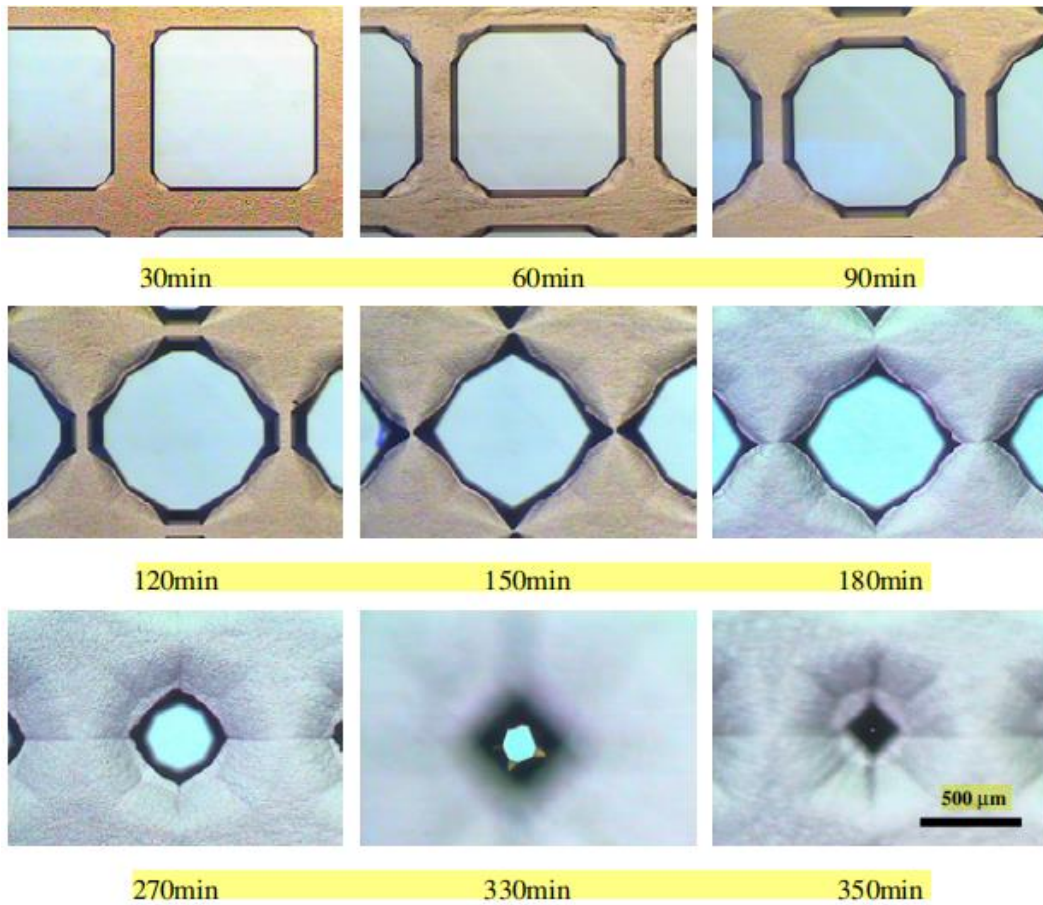


Figure 1.4.2 [25] Microscope image of microneedle mask over increasing KOH etching time (topview). Blue area representative for the SiN<sub>x</sub> mask; Brown area representative for bare silicon.

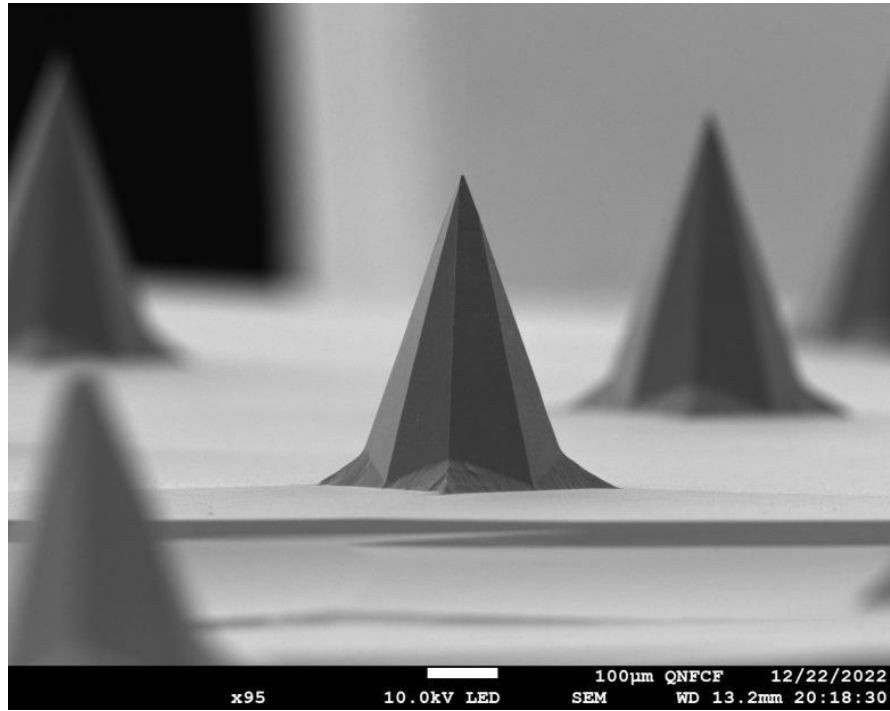


Figure 1.4.3 SEM image of microneedles array fabricated by KOH wet etching.

## 2. Experiments

Experiments part consists of the materials and equipment used during microneedles fabrication, and recipes used in every steps. Experiments are introduced following the order of fabrication process flow.

(100) Oriented silicon wafers with thickness of 1000  $\mu\text{m}$  are used as substrate; 29wt% of KOH solution diluted from 45wt% KOH solution is used as etchant in this thesis. During the fabrication process, low pressure chemical vapor deposition (LPCVD), spin-coater, maskless aligner (MLA), reactive ion etching (RIE), and water bath machines are used. Ellipsometer, filmetrics, optical microscope and scanning electron microscope (SEM) are used for characterization.

### 2.1 $\text{SiN}_x$ thin film deposition and mask patterning

200nm of  $\text{SiN}_x$  is deposited on silicon wafers by LPCVD to achieve double-side deposition and high resistance against KOH etching. Dichlorosilane ( $\text{SiCl}_2\text{H}_2$ ) and ammonia ( $\text{NH}_3$ ) gas are used as reactant gases to form  $\text{SiN}_x$  film [26]. The  $\text{SiN}_x$  film thickness and film uniformity are characterized by filmetrics (Figure 2.1.1).

Square-shaped masks with sidewall following  $\langle 100 \rangle$  direction and  $\langle 110 \rangle$  direction with various size are designed using the software Klayout. The saved .GDS file can be directly used in MLA for lithography.

The mask patterning is achieved by lithography and reactive ion etching. First, UV photoresist S1811 is spin-coated on wafer at 3000RPM for 30s , and baked for 120s on

hotplate at 120°C. Then, lithography is carried by using MLA. The light source is chosen at 375nm; Dose is chosen as 105 mJ/cm<sup>2</sup>. Since S1811 is a positive resist, designed mask pattern has to be inverted to get the correct mask pattern. Development is performed to dissolve the exposed resist by soaking in developer MF-319 for 60s.

Finally, pattern on resist is transferred onto SiN<sub>x</sub> film by reactive ion etching. The etching recipe is shown in Table 1. Etching time is set to 3 minutes to get a complete etching of SiN<sub>x</sub>. After SiN<sub>x</sub> etching, the sample is ready for wet etching. Figure 2.1.2 shows the shape of designed digital mask and real SiN<sub>x</sub> mask.

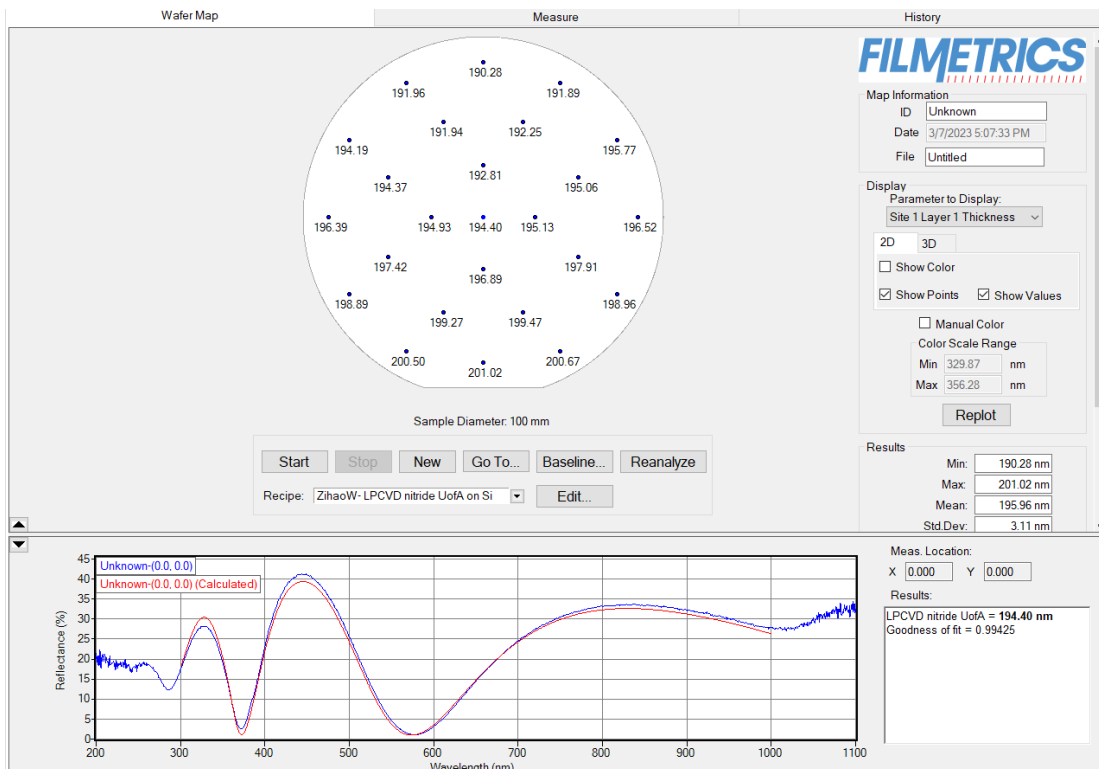


Figure 2.1.1 SiN<sub>x</sub> thickness map by filmetrics.

Table 1. Reactive ion etching recipe for SiN<sub>x</sub> etching.

Time (s)	Temp (°C)	Pressure (mTorr)	RF (W)	ICP (W)	CHF <sub>3</sub> (sccm)	O <sub>2</sub> (sccm)	V-dc (v)
100	20	5	100	500	50	5	50

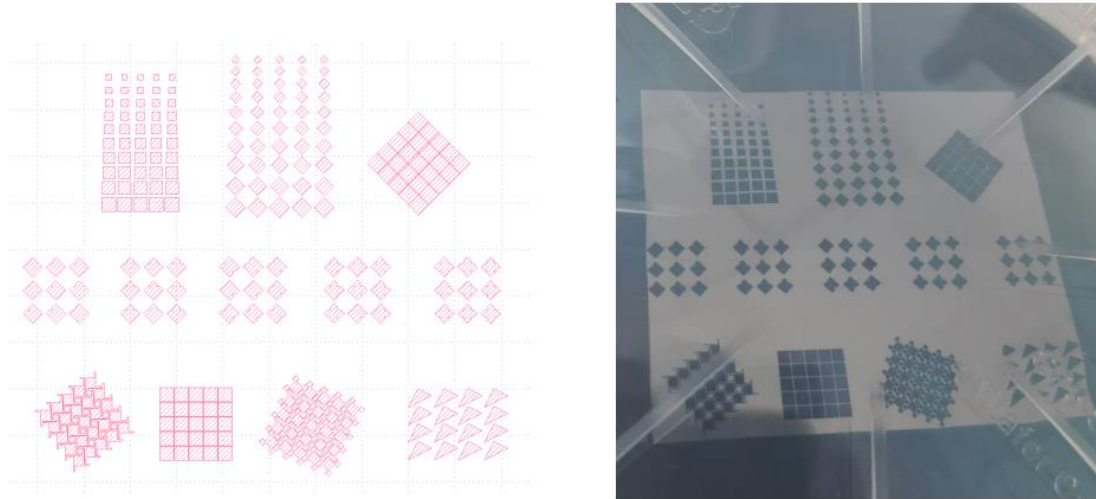


Figure 2.1.2. Left: Layout of parts of designed masks; Colored area represent for SiN<sub>x</sub> mask. Right: SiN<sub>x</sub> mask on Si wafer; Blue area represent for SiN<sub>x</sub> mask.

## 2.2 KOH etching

When the SiN<sub>x</sub> mask is patterned on Si wafer, KOH etching can be carried out. As mentioned, 29wt% potassium hydroxide solution is used as etchant to anisotropically etch silicon. Etching temperature is set at 79 degree Celsius. In order to accurately control the

temperature, a water bath equipment is needed, which can automatically keep a uniform temperature within the water bath.

Sufficient KOH solution is added in beaker and heated by water bath until temperature of KOH solution is stable at 79°C, while the water bath temperature is 84°C. When temperature of KOH solution is stable at 79°C, sample is put in the solution with the pattern facing up. Bubbles come out within a few seconds, which means the Silicon etching process has been started. Last but not least, a beaker cover is an important component in the etching system, which can dramatically reduce the solution evaporation and heat loss. Figure 2.2.1 shows the KOH etching system including the water bath equipment, beaker, and beaker cover, as well as a sample being etched in KOH solution.

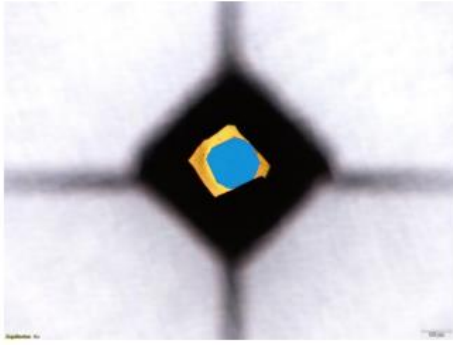
Finally, the KOH etching process is considered finished when the SiN<sub>x</sub> mask on top falls off. The stop point can be determined under optical microscope by observing color difference between SiN<sub>x</sub> mask and silicon. Figure 2.2.2 shows the microscope image of microneedles with insufficient etching and sufficient etching, and the SEM image of microneedles when the mask and reverse structure is just about to fall. In (a), the blue area represents the SiN<sub>x</sub> mask; The gray area is silicon substrate; The yellow area indicates the protruded SiN<sub>x</sub> mask without underneath silicon; The black area stands for microneedles structure due to poor reflection from sidewall to microscope, which also proves that smooth sidewalls are formed during KOH etching. Generally, due to the existence of reverse silicon structure, the mask will fall off when mask size shrinks to less than 20 μm approximately for 500 μm high microneedles.



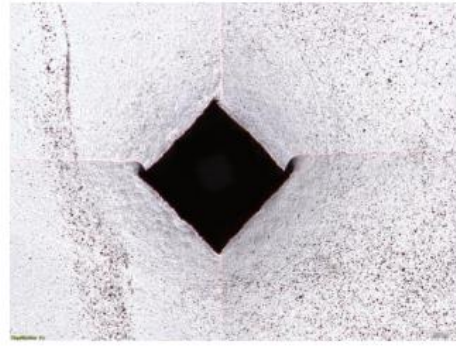
(a)

(b)

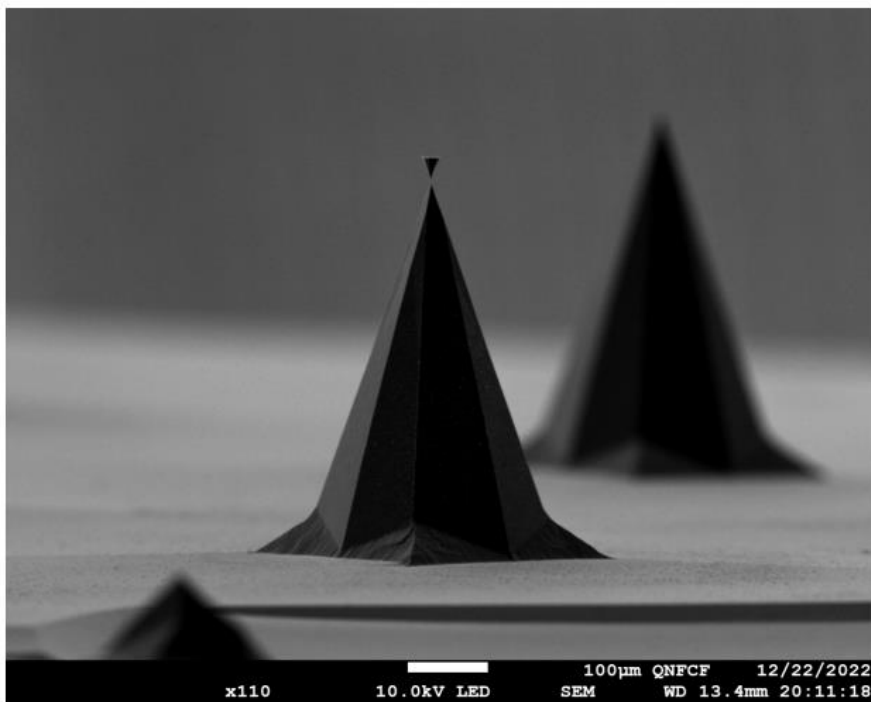
Figure 2.2.1. (a) KOH etching system, including water bath equipment, beaker, and beaker cover. (b) Sample under KOH etching, with hydrogen bubbles coming out.



(a)



(b)



(c)

Figure 2.2.2 (a) Topview of microneedles with insufficient etching; (b) Topview of microneedles with sufficient etching. (c) SEM image of microneedles with reverse structure on top.

### 2.3 Reactive ion etching by using SF<sub>6</sub>

The purpose of this step is to improve the height uniformity of microneedles within array and the tip sharpness of microneedles. To achieve this purpose, KOH etching step is stopped when SiN<sub>x</sub> mask has 10 μm to 30 μm remaining, before falling off. The reactive ion etching by using SF<sub>6</sub> gas is carried out to finally etch the microneedles. SF<sub>6</sub> is chosen because its etching of silicon is isotropic with significant lateral etching. The mask will fall off when the narrowest neck (located slightly below the mask) is laterally etched through. Table 2 shows the reactive ion etching recipe for final microneedles etching. The silicon etching rate using this recipe is 2.5 μm/min.

Table 2. Reactive ion etching recipe for Si isotropic etching

Recipe: OPT Si isotropic etch								
Step	Time (s)	Temp (oC)	Pressure (mTorr)	RF (W)	ICP (W)	SF <sub>6</sub> (sccm)	O <sub>2</sub> (sccm)	V-dc (V)
1min pump	60	5	-	-	-	-	-	-
Strike	3	5	10	50	2000	-	60	-
Si etching	60	5	10	50	2000	45	-	90
1min pump	60	5	-	-	-	-	-	-

## 2.4 Characterization of microneedles structure

When the microneedle fabrication process is finished, microneedles structure on silicon wafer can be clearly seen by eyes (Figure 2.4.1). In order to characterize the structure of microneedles, optical microscope is used to monitor the KOH etching process to make sure the etching is sufficient; Scanning electron microscope (SEM) is used to observe the structure and measure the dimension of microneedles in low magnification range, and characterize the tip structure in high magnification range.

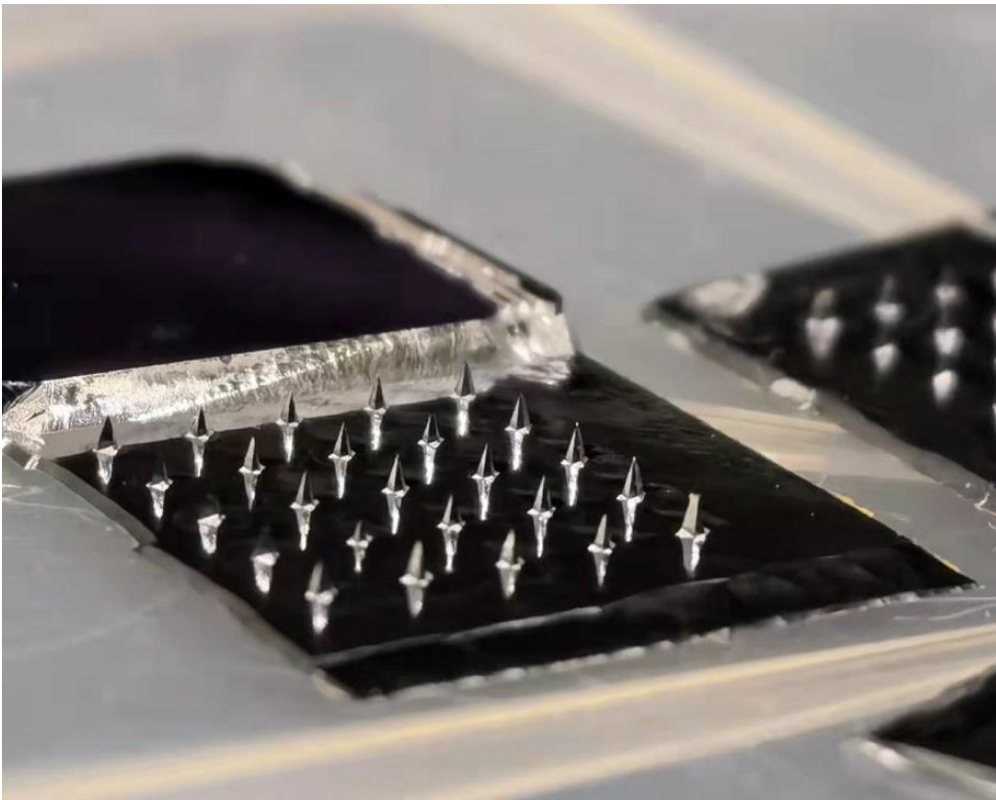


Figure 2.4.1 Phone photo of microneedles array.

### 3. Results & Discussion

In the results and discussion part, the KOH etching model is established including anisotropy of etching rate, geometry of microneedles structure during etching process, relations between microneedles height versus mask size and etching time. Moreover, SF<sub>6</sub> RIE step is carried to minimize the random error in etching process, which can improve the height uniformity and tip sharpness of microneedles.

#### 3.1 Geometry of microneedles and anisotropy of KOH wet etching.

The structure of microneedles fabricated by KOH wet etching is shown as an octagonal pyramid in shape, with a short protruded base structure at bottom. (Figure 3.1.1)

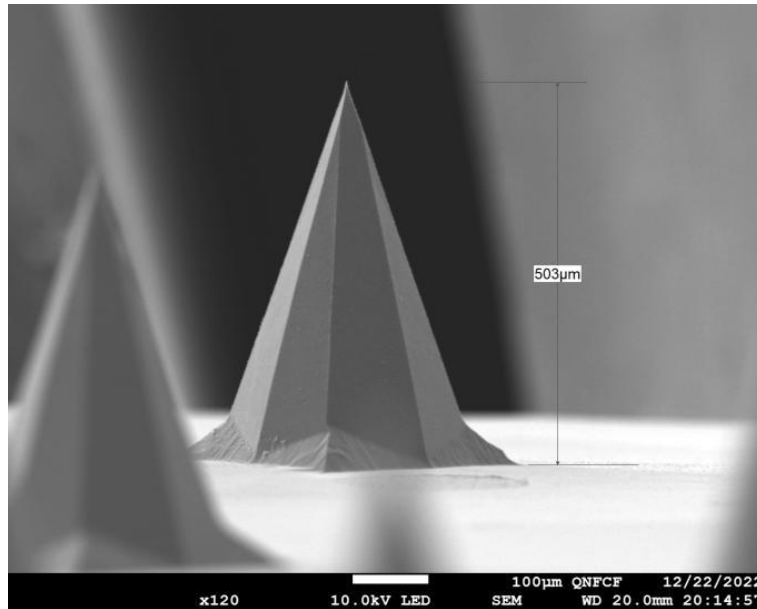


Figure 3.1.1. SEM image of microneedles by KOH etching. Height of microneedle is measured as 503 μm.

As mentioned in introduction part, the microneedles structure is formed based on the different silicon etch rate on different crystalline planes. The sidewalls are the fastest etching planes which can be determined by measuring the angle between different planes from topview and sideview. Figure 3.1.2 shows the SEM images of topview and sideview of microneedles structure. Angles between nearby planes are measured to determine the crystalline planes. From sideview projection, the angle between ground surface (100) and microneedle structure is measured as 71.7 degree. From topview projection,  $\beta_1$  is measured as 127 degree and  $\beta_2$  is measured as 143 degree. By comparing the angles with theoretical data, (311) plane is considered as sidewall plane because it has the closest angles to experimental results, which is 71.56 degree from  $\langle 100 \rangle$  projection, 126.87 degree and 143.13 degree as  $\beta_1$  and  $\beta_2$  respectively from topview projection. Thus, Moreover, the aspect ratio is 1.41 by measurement, which is also close to theoretical number of 1.414.

In order to get anisotropy of microneedle etching, etching rate of (100) plane and (311) plane need to be determined. Etching rate of (100) plane can be directly measured as 72.5  $\mu\text{m}/\text{h}$ . Etching rate of (311) plane can be calculated from mask shrinking rate which is measured as 298  $\mu\text{m}/\text{h}$  and the angle between (311) plane and ground, which is 72.45 degree. Thus the etch rate of (311) plane  $r_{(311)}$  :

$$r_{(311)} = \frac{298/2}{\sin(72.45^\circ)} = 156.3 \text{ um/hr}$$

Etch rate of (311) plane is much faster than etch rate of (100) plane, which is reasonable as (311) plane is supposed to be the fastest etching plane during the etching

process. Moreover, by combining the etch rate of (100) and (311) and the angle between (100) and (311), the overetching rate can be calculated:

$$r_{OE} = \frac{r_{(311)}}{\cos(72.45^\circ)} - r_{(100)} = \frac{156.3}{\cos(72.45^\circ)} - 72.5 = 445.8 \text{ } \mu\text{m/hr}$$

The over etching rate refers to the dropping rate of microneedles height after falling off of SiN<sub>x</sub> mask. Obviously, over etching rate is about five time faster than etch rate of (100) plane, which means the over etching has to be critically controlled to within a very short time to protect the microneedles from fast height dropping. However, the measured over etching rate is 400 μm/h, which is 10% smaller than calculated over etch rate. Possible reason for the difference is that the etching is non-uniform within whole substrate and also within bulk KOH solution.

In summary, the geometry of microneedles and anisotropy of etching rate in 29% KOH solution at 79°C are obtained. The microneedle is an octagonal pyramid shape with eight (311) planes as sidewalls. The aspect ratio of microneedles is 1.4 by measurement, and 1.414 by theoretical calculation. The anisotropic etch rate of (100) plane is measured as 72.5 μm/h; Etch rate of (311) plane is calculated as 156.3 μm/h from mask shrinking rate; Over etching rate is 400 μm/h by measurement, and 445.8 μm/h by calculation from mask shrinking rate. 10 percent of error occurs in measurement due to the non-uniform etching rate and SEM calibration and measurement accuracy. All the measured and calculated results are summarized in table 3.

Table 3. Measured and calculated etching rate of different plans and aspect ratio of microneedles.

	measured	calculated
Etch rate of (100)	72.5 $\mu\text{m}/\text{h}$	N/A
Etch rate of (311)	N/A	156.3 $\mu\text{m}/\text{h}$
Over etching rate	400 $\mu\text{m}/\text{h}$	445.8 $\mu\text{m}/\text{h}$
Aspect ratio	1.40	1.414

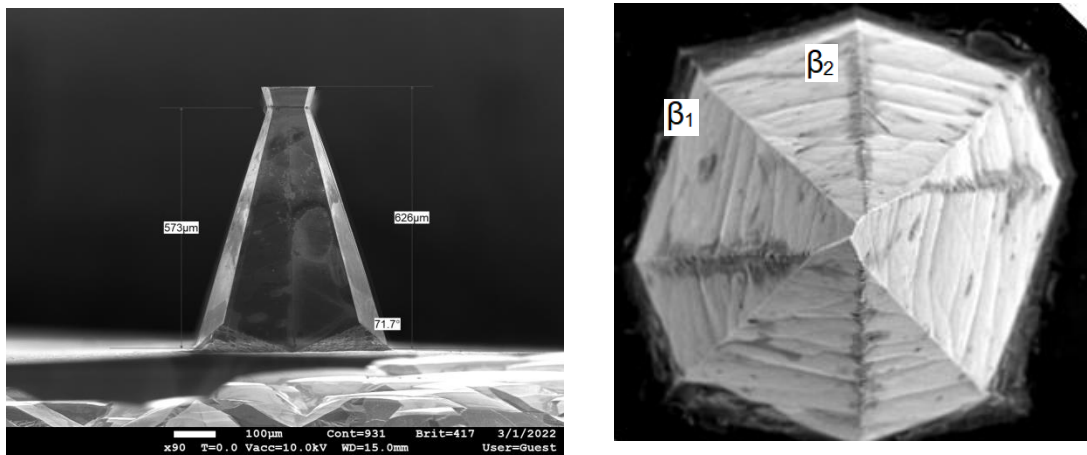


Figure 3.1.2 SEM image of microneedle. Sideview of microneedle with insufficient etching from  $\langle 100 \rangle$  direction (left). Topview of microneedle with sufficient etching (right).  $\beta_1$  indicates the top-left angle;  $\beta_2$  indicates the top angle.

### **3.2 Relationship between microneedles height versus mask size and etching time.**

In order to control the microneedles height, a model that simulates the formation process of microneedles is necessary to predict the behavior of microneedles. The microneedles height is affected by many factors such as mask shape, mask size, etchant and its concentration, and etching temperature. In this experiment, mask shape, etchant and its concentration, as well as etching temperature are fixed. Thus, except of fixed parameters, the mask size can be chosen as variable to study the relationship between the microneedles height and mask size. Moreover, the etching is a dynamic process and the height of microneedles structure also depends on the etching time. By studying the relationship between real-time microneedles height versus etching time, the actual real-time microneedle height can be calculated based on etching time and mask size.

To achieve this goal, a gradient of  $\text{SiN}_x$  mask size from 600  $\mu\text{m}$  to 1500  $\mu\text{m}$  with step size of 100  $\mu\text{m}$  is designed. The sample is etched in KOH solution and measured at multiple time spots. Figure 3.2.1 shows the layout of the mask design and the  $\text{SiN}_x$  mask after reactive ion etching, as well as the SEM image after KOH etching. As seen in figure 3.2.1 (c)(d), by measuring the microneedles heights at different times, the relationship between the microneedles height versus mask size and etching time can be obtained. Note that the first left column of microneedles are considered to be overetched, with a huge height dropping compared to others; second left column of microneedles are considered just well etched; Other columns of microneedles are considered insufficiently etched with

mask still on top. Table 4 shows the microneedles (structure) height with various mask size and different time.

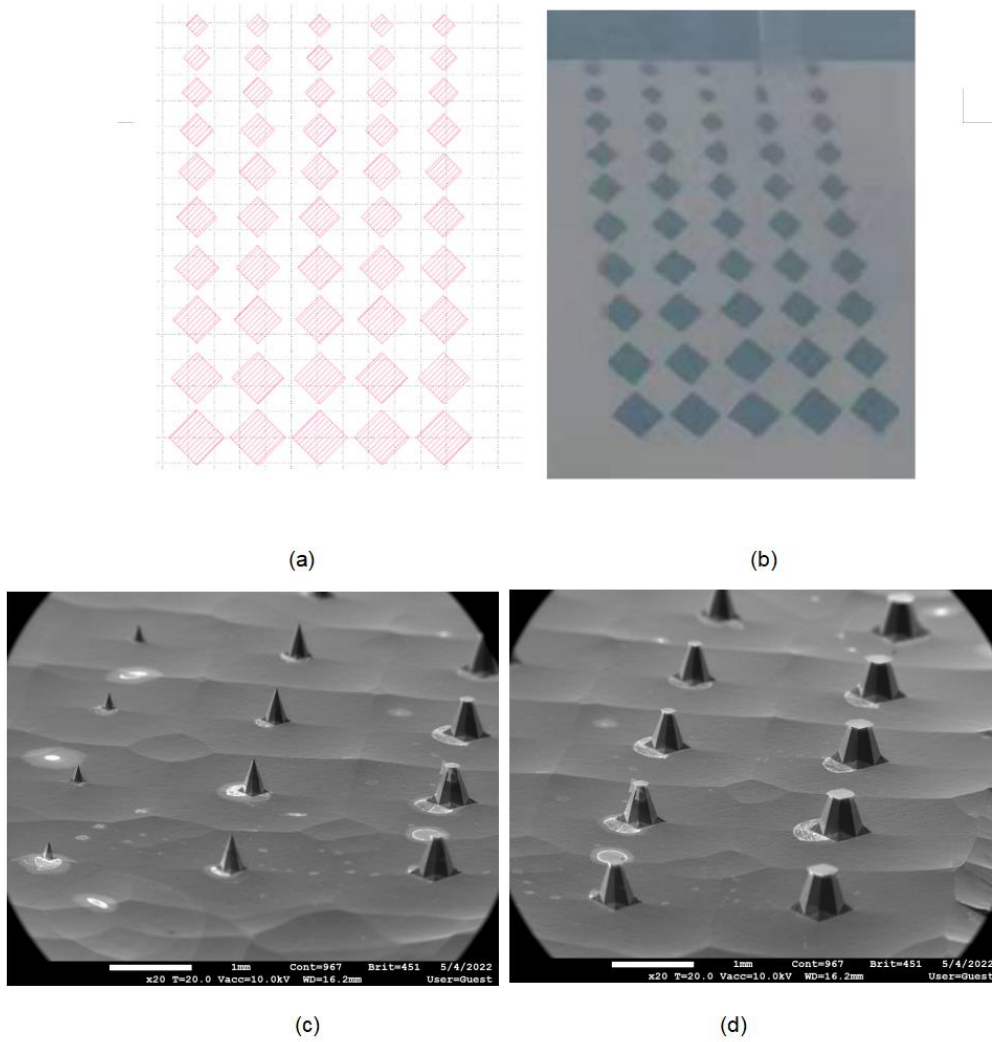


Figure 3.2.1. (a) Layout of SiN<sub>x</sub> mask shape and size. (b) SiN<sub>x</sub> mask after reactive ion etching. Blue area indicates SiN<sub>x</sub>. (c)(d) SEM images of microneedles. Mask size of microneedles is increasing from left to right.

Table 4. Microneedles height from variety of mask sizes and etching time. (microneedles with mask size less than 900um are etched over, thus data is not shown in table)

Original mask sidelength ( $\mu\text{m}$ )	Microneedles height		
	( $\mu\text{m}$ )		
1500	350	435	472
1400	350	435	409
1300	350	410	210
1200	350	190	0
1100	350	0	0
1000	210	0	0
900	20	0	0
<b>Etching time</b>	<b>5h</b>	<b>6h</b>	<b>6.5h</b>

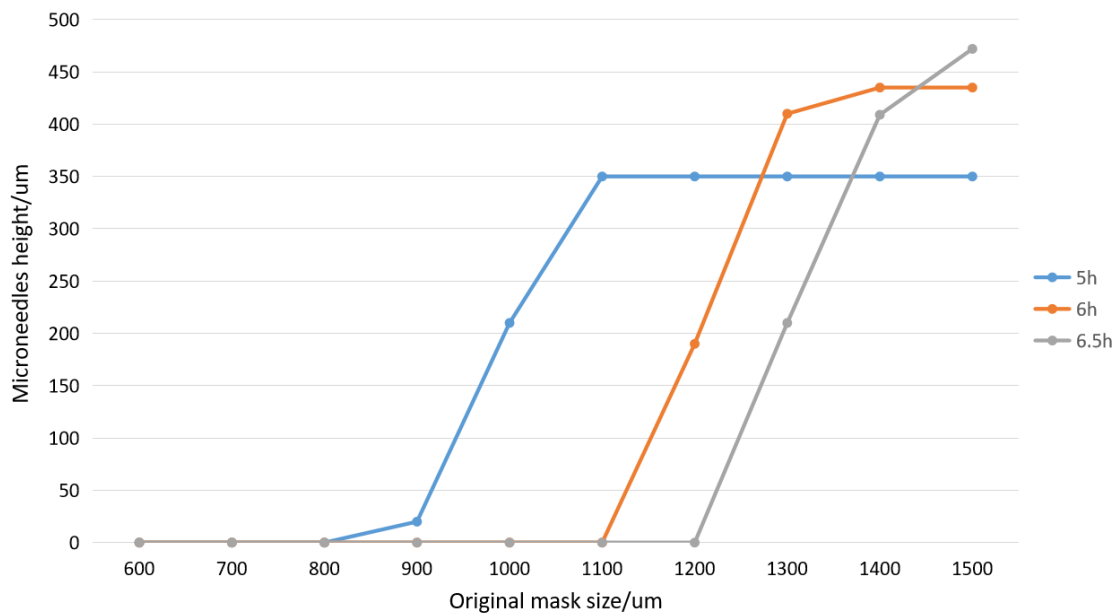


Figure 3.2.2. Diagram of microneedles height versus original mask size with etching time 5h (blue curve), 6h (orange curve), 6.5h (gray curve). (Data from table 4)

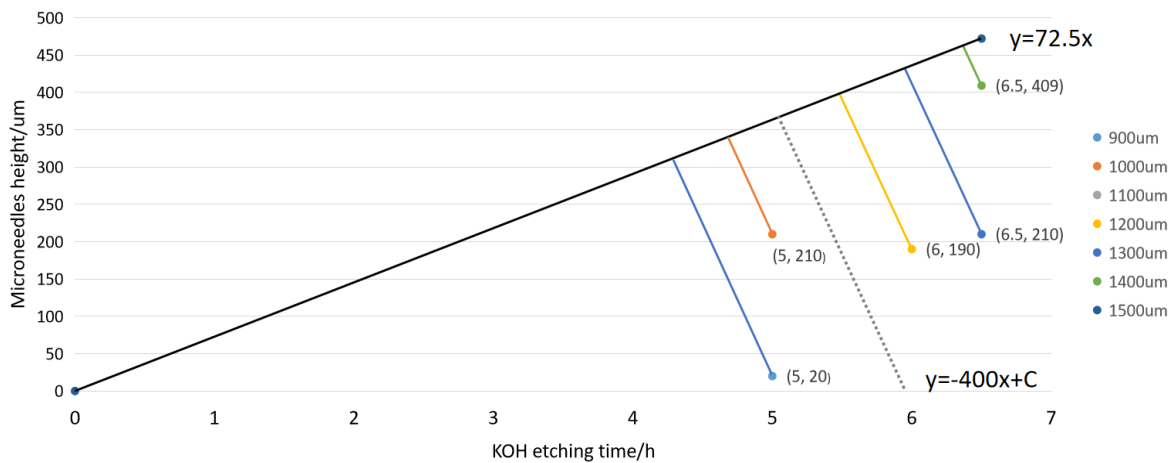


Figure 3.2.3. Diagram of microneedles height versus etching time. Black line represent the growth stage of microneedles. Colorful lines indicate the overetching stage of microneedles with variety of original mask sidelength. (Data from table 4)

By plotting the data in table 4 into diagrams, the correlation between maximum microneedles height and original mask size as well as the correlation between real-time microneedles height and etching time can be calculated. In figure 3.2.2, the left parts of the curves represent the stage that the microneedles already disappeared due to over etching, where the microneedles height is zero. The center parts of curves where the microneedles height is increasing represents the stage that microneedles are already formed and under overetching. The right parts of curves represent the stage that the microneedles still have mask on top, where the microneedles height keeps constant. The center parts of the curves where the slope is nearly constant shows that the difference in microneedles height is proportional to the difference in original mask size, indicating that the maximum microneedles height that a mask can support, is also proportional to its original mask sidelength. Thus, the etching time that a mask can sustain is also proportional to its original mask sidelength since all microneedles share the same etching rate. In order to get the

relationship between real-time microneedles height and etching time, the turning point where the mask falls off and the overetching starts has to be found. Figure 3.2.3 aims to calculate the turning point where the microneedles attain the maximum height. Since the microneedles growth rate and overetching rate are known as 72.5  $\mu\text{m/h}$  and 400  $\mu\text{m/h}$  respectively, only one point is needed to determine the intersection point of growing and overetching, when is exactly the moment that microneedles attain the maximum height. Thus, by measuring the height of a microneedle at a moment during overetching stage, the moment that the microneedle attain its maximum height can be calculated, which is  $t=0.00465L$ . where  $t$  is the etching time in unit of hour. And the relationship between maximum microneedles height ( $H$ ) and mask sidelength ( $L$ ) can be expressed as:

$$H=0.32L$$

The real-time microneedles height ( $h$ ) can be expressed by the etching time ( $t$ ):

$$\begin{array}{ll} h=72.5t & \text{when } t \leq 0.00465L \\ h=0.32L-400(t-0.00465L) & \text{when } t > 0.00465L \end{array}$$

Note that due to the reverse structure on top of microneedles structure (seen in figure 3.1.2), which is around 5% of total microneedles height, the maximum microneedles height is slightly less than the etching depth on (100) plane. 5% correction has been applied in equations to get a more accurate result.

From these relationships, the behavior of microneedles during KOH etching can be explained: At beginning, microneedles grow at a rate of 72.5  $\mu\text{m/h}$  until the  $\text{SiN}_x$  mask

falls, at which time the microneedles reach the maximum height. Then overetching starts and the microneedles suffer a fast rate of height dropping at 400um/hr. Finally with a long time of overetching, no microneedle structure is left.

In summary, the behavior of microneedles during KOH etching process is revealed and a model of microneedles height versus mask size and etching time is established. Based on the model, the desired microneedles height can be obtained by mask design and etching time control, which can dramatically simplify the mask design process and reduce the characterization time for height measurement. Also, the proper time of KOH etching process can be estimated, which can help to avoid unwanted overetching.

### **3.3 Microneedles height uniformity and tip sharpness improvement by SF<sub>6</sub> reactive ion etching.**

In theory, the fabrication process of microneedles by KOH etching is simple and reproducible. The shape of microneedles should follow the crystalline structure and the etch rate of different planes should be well defined based on the anisotropic properties. As a result, the final microneedles structure should be perfect in geometry and uniform within the whole substrate. However, it does not follow the theory when coming into practice. In fact, the structure of fabricated microneedle is not perfect octagonal pyramid. And the height of microneedles is not consistent within one sample. Figure 3.3.1 shows a microneedles array that has a poor height uniformity. Several possible causes for the non-uniformity of microneedles height are revealed:

1. Local temperature difference and the produced hydrogen bubbles affect the local etch rate, resulting in the difference of microneedles height. Even the temperature is controlled by water bath equipment, the temperature of KOH solution cannot achieve perfect uniformity.

2. Defects of  $\text{SiN}_x$  film lead to the leakage of mask. In theory, 200nm  $\text{SiN}_x$  mask can resist more than 100 hours of KOH etching. However, a large area of mask was occasionally torn off after 10 hours of etching. Figure 3.3.2 (a) shows a large area that already etched through due to poor  $\text{SiN}_x$  mask quality, while the remaining mask at other area is still 190nm thick. The  $\text{SiN}_x$  film at backside is easier to get destroyed than front side, which can breakdown the base of microneedles and damage the whole sample.

3. Mis-matching of silicon crystalline structure in silicon wafer causes the change of microneedles geometry. Figure 3.3.2 (b) shows the wafer surface after KOH etching. Ring structure can be observed that shares the center with the circular wafer. The ring may come from the pulling process in wafer manufacture by CZ method or from the polishing step. As a result, the microneedles growing on the ring may have poor crystalline structure, which leads to shorter height.

4. The local native oxide can participate as temporary etching mask to resist the etching. The native oxide exists on the interface between  $\text{SiN}_x$  film and silicon substrate, and have a high KOH etching resistance. Thus, the shrinkage rate of  $\text{SiN}_x$  mask will be locally different and result in a less symmetric microneedles shape.

5. When it comes to high microneedles fabrication (500  $\mu\text{m}$ ), seven hours etching make the non-uniformity more serious than fabricating shorter microneedles.

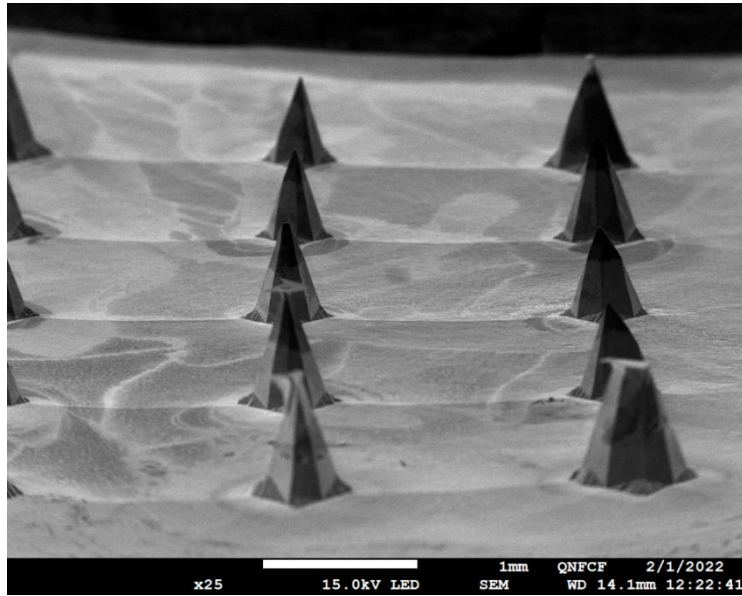


Figure 3.3.1. SEM image of microneedles with poor height uniformity.



(a)

(b)

Figure 3.3.2. Silicon substrate phone photos after long time KOH etching. (a) Backside of substrate piece with damaged area. (b) Frontside of a half wafer, with ring structure shown under light reflection.

As a consequence, it is important to find out a way to minimize the microneedles height error from these uncontrollable factors.

As introduced, the overetching rate after mask falling is 400  $\mu\text{m}/\text{h}$ , which is 5 times faster than microneedles etching rate. If the mask falls at different moment due to the non-uniform shrinking rate of  $\text{SiN}_x$  mask, the overetching will start at different moment, which can cause a great height difference at last. However, before the mask falling, the microneedles maintain the same height, which only depends on the etch rate of (100) plane. Therefore, by controlling the mask falling time the same among microneedle array, the height difference can be minimized.

A following step of reactive ion etching (RIE) is introduced to finally etch away the mask, instead of finishing the etching by KOH wet etching. The KOH etching is stopped when most of microneedles have their masks on top, at which moment microneedles have nearly the same height. The remaining mask size varies from 10  $\mu\text{m}$  to 50  $\mu\text{m}$  for 500  $\mu\text{m}$  high microneedles, which needs about 5-minutes reactive ion etching to complete the microneedles structure.

Figure 3.3.3 shows the SEM images of microneedles array before and after 5 minutes  $\text{SF}_6$  reactive ion etching. As seen, microneedles received insufficient etching before RIE, then achieved a sharp needle structure after RIE. The heights of 12 microneedles in an array finished by additional RIE are measured, and compared with height of 12 microneedles in an array with same mask design that are finished by KOH etching to determine if the height uniformity is improved by additional  $\text{SF}_6$  RIE step. Table 5 shows all the measured height of microneedles fabricated by KOH only and KOH +  $\text{SF}_6$ . Figure 3.3.4 shows the diagram of average height and its standard deviation of microneedles

etched by KOH only, or KOH plus SF<sub>6</sub> RIE step. For the microneedles etched by KOH only, the average height and its standard deviation are 429.25 μm and 20.50 μm respectively; For the microneedles etched by KOH plus additional SF<sub>6</sub> etching, the average height and its standard deviation are 477.5 μm and 11.12 μm respectively. It is obvious that the microneedles etched by KOH plus additional SF<sub>6</sub> etching have a larger average height and less height variation, which means that the additional SF<sub>6</sub> RIE step can not only keep the microneedles as tall as possible, but also improve the height uniformity. Because the SF<sub>6</sub> RIE etching is isotropic etching, which results in a similar etching rate among different directions, the fast over-etching rate for KOH over-etch does not happen in this case. The lateral etching gradually thins down the narrowest neck until mask falls down, and then vertical etching occurs on both tip and base of microneedles. During SF<sub>6</sub> isotropic etching, the height dropping rate after mask falling off is measured as 144.1 μm/h, which is comparable to the Si etching rate using RIE; while during KOH etching, the height dropping rate after mask falling off is measured as 400um/hr, which is roughly five times of the Si etching rate by KOH. Thus, compared to KOH over-etching, over-etching using SF<sub>6</sub> RIE is more controllable as it will result in less height drop and consequently less height variation among microneedles.

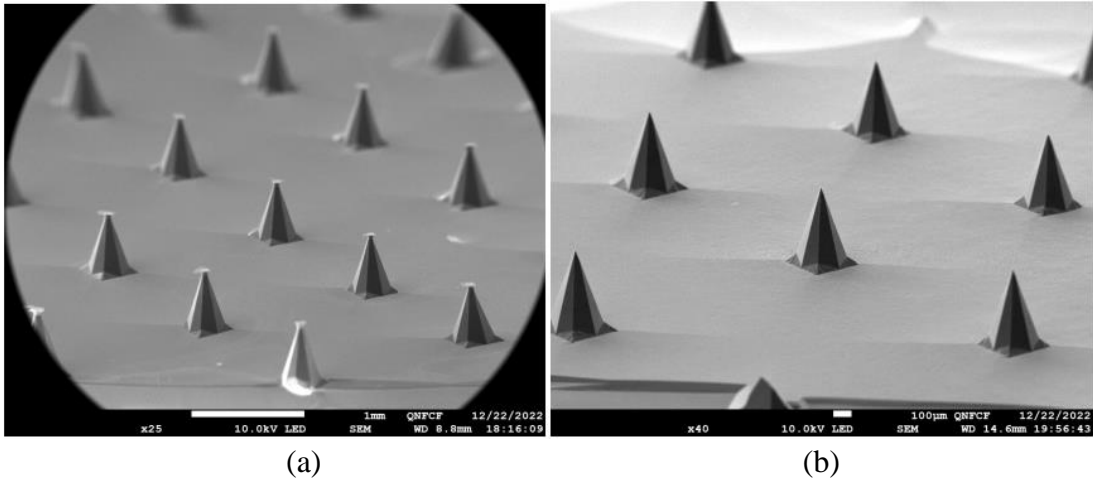


Figure 3.3.3 SEM images of microneedles array (a) before SF<sub>6</sub> RIE, and (b) after SF<sub>6</sub> RIE.

Table 5. Raw data of microneedles height and tip blade length

Microneedles height (um)	KOH	434, 462, 453, 431, 401, 412, 428, 406, 403, 455, 447, 418
	KOH+SF <sub>6</sub>	462, 464, 461, 466, 477, 474, 485, 491, 491, 485, 487, 487
Tip blade length (um)	KOH	1.53, 8.85, 11.5, 8.32, 5.89, 9.78, 10.9, 6.28, 5.36, 7.89, 4.95, 1.83
	KOH+SF <sub>6</sub>	2.67, 3.73, 4.22, 4.46, 4.26, 3.81, 0.74, 0.83, 3.08, 1.22, 2.62, 0.88

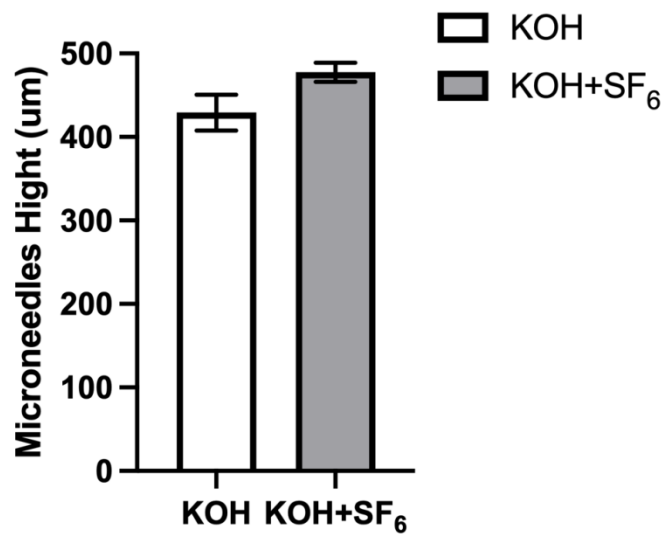


Figure 3.3.4. Diagram of height of microneedles fabricated by KOH only, and KOH + SF<sub>6</sub> etching.

Besides, the tip sharpness of microneedles is also an important property, which can dramatically affect the penetration efficiency of microneedle product. In theory, microneedles fabricated by KOH etching can achieve atomic level tip sharpness because the tip structure is determined by crystalline orientation. However, in practice, the eight sidewalls are hard to focus onto one point to achieve atomic level sharpness, especially when fabricating taller microneedles. Most of tips of microneedles show a blade structure instead of sharp tip due to the non-symmetric structure of sidewalls. Figure 3.3.5 shows the SEM image of typical blade-shape tip with blade length more than 10  $\mu\text{m}$ , and nearly perfect tip with tip sharpness less than 1  $\mu\text{m}$ . From Figure 3.3.5(a), there are two sidewalls dominating the top and forming the blade structure, while other sidewalls are less etched, leaving a distance from opposite sidewall, which is exactly the blade-shape tip.

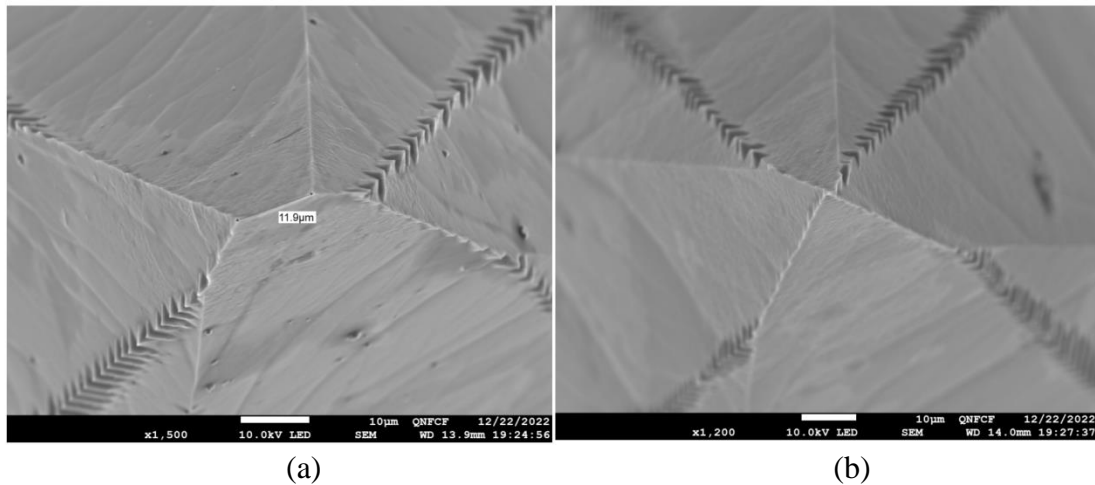


Figure 3.3.5 Topview SEM image of microneedle tip. (a) typical blade-shape tip with blade length=11.9  $\mu\text{m}$ . (b) Sharp tip with tip diameter less than 1  $\mu\text{m}$ .

SF<sub>6</sub> RIE step can also help to reduce the blade size by making the microneedle more rounded. The tip blade length of 12 microneedles fabricated by KOH plus SF<sub>6</sub> etching is measured, and compared with 12 microneedles with same mask design fabricated by KOH etching only (table 5). Figure 3.3.6 shows the tip diameter and its standard deviation of microneedles fabricated by KOH etching only, as well as KOH plus SF<sub>6</sub> etching. For the microneedles fabricated by KOH etching, the average tip diameter and its standard deviation are 6.92 μm and 3.09 μm respectively; For the microneedles fabricated by KOH etching and SF<sub>6</sub> etching, the average tip diameter and its standard deviation are 2.71 μm and 1.39 μm respectively.

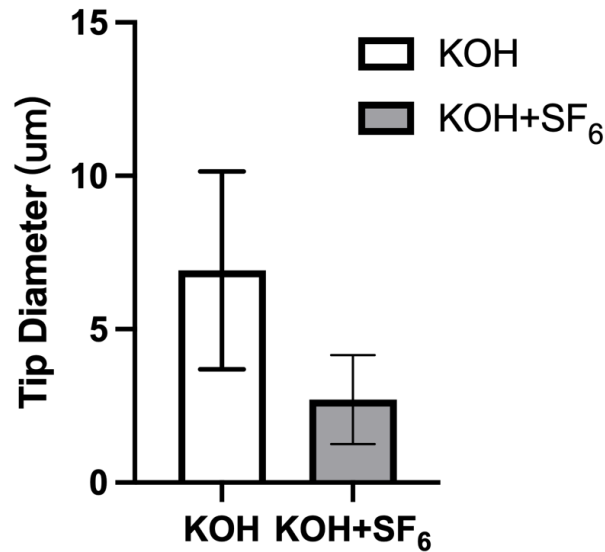


Figure 3.3.6. Diagram of tip diameter of microneedles fabricated by KOH only, and KOH + SF<sub>6</sub> etching.

In summary, in order to improve the height uniformity of microneedles, SF<sub>6</sub> reactive ion etching is introduced after KOH etching to finally complete the microneedles structure. By dramatically reducing the height dropping rate during over etching, the height

uniformity has a great improvement. Moreover, SF<sub>6</sub> etching also helps to improve the tip sharpness by reducing the length of blade-shape tip structure.

## 4. Conclusions

The fabrication and characterization process of solid silicon microneedles, as well as the height uniformity and tip sharpness improvement method are presented in this thesis.

First, the geometry of microneedles structure is determined, and the anisotropy of KOH wet etching is studied. For etching in 29wt% KOH solution at 79°C, the microneedle is an octagonal pyramid shape with eight (311) planes as sidewalls. The etch rate of (100) plane is measured as 72.5  $\mu\text{m/h}$ ; The etching rate of (311) plane is calculated as 156.3  $\mu\text{m/h}$ ; The height dropping rate during KOH over etching is 400  $\mu\text{m/h}$ .

Second, based on the geometry of microneedles and etch rates of planes, an etching model is established to explain the relationship between the microneedles height versus the mask size and KOH etching period. The maximum microneedles height for a given mask is proportional to the mask size; The real-time microneedles height has a positive then negative correlation versus KOH etching time, which allows to predict the growth of microneedles based on mask size and etching time.

Finally, in order to improve the height uniformity among microneedles array,  $\text{SF}_6$  reactive ion etching is introduced at final stage of KOH etching. The additional  $\text{SF}_6$  etching step can improve the height uniformity, by decreasing the STDV of microneedles height from 20.50  $\mu\text{m}$  to 11.12  $\mu\text{m}$ . It can also improve the tip sharpness by decreasing the average tip diameter from 6.92  $\mu\text{m}$  to 2.71  $\mu\text{m}$ .

However, the next-level research is needed in the future to characterize the properties of the microneedles such as mechanical strength, conductivity, as well as the properties in vivo during skin penetration, such as how the structure of microneedles and its surface roughness affect the penetration and wound recovery. Moreover, based on microneedles,

the device for drug administration or biosensing can be fabricated and characterized in order to achieve practical applications.

Overall, the work has a strong practical significance in microneedle fabrication. The growth of microneedles can be controlled quantitatively during KOH wet etching, which contributes to the saving of material and time cost. The optimization of height uniformity and tip sharpness improves the quality of microneedles product and make it more competitive in microneedles market.

## References

- [1] Feynman. (2011). There's plenty of room at the bottom: An invitation to enter a new field of physics. *Resonance*, 16(9), 890–904.
- [2] Habiba, Makarov, Weinel, Morell. 2014
- [3] D. Mijatovic, J. C. T. Eijkel, A. van den Berg. (2015). “Technologies for nanofluidic systems: top-down vs. bottom-up—a review,” *Lab Chip*, vol. 5, no. 5, p. 492, 2005. .
- [4] Madou. (2011). *Fundamentals of Microfabrication and Nanotechnology, Three-Volume Set* (Third edition.). CRC Press
- [5] Tirapu Azpiroz, & Rosenbluth, A. E. (2013). Impact of sub-wavelength electromagnetic diffraction in optical lithography for semiconductor chip manufacturing. *2013 SBMO/IEEE MTT-S International Microwave & Optoelectronics Conference (IMOC)*, 1–5.  
<https://doi.org/10.1109/IMOC.2013.6646420>
- [6] Langer. (1990). *New Methods of Drug Delivery*. Science (American Association for the Advancement of Science),
- [7] Waghule, Singhvi, G., Dubey, S. K., Pandey, M. M., Gupta, G., Singh, M., & Dua, K. (2019). Microneedles: A smart approach and increasing potential for transdermal drug delivery system. *Biomedicine & Pharmacotherapy*, 109, 1249–1258.  
<https://doi.org/10.1016/j.biopha.2018.10.078>
- [8] Kim, Park, J.-H., & Prausnitz, M. R. (2012). Microneedles for drug and vaccine delivery. *Advanced Drug Delivery Reviews*, 64(14), 1547–1568.  
<https://doi.org/10.1016/j.addr.2012.04.005>
- [9] Milani, R. V. & Lavie, C. J. Health care 2020: reengineering health care delivery to combat chronic disease. *Am. J. Med.* 128, 337–343 (2015).
- [10] Zheng, Y. et al. Global aetiology and epidemiology of type 2 diabetes mellitus and its complications. *Nat. Rev. Endocrinol.* 14, 88–98 (2018)
- [11] Liu, Yu, Q., Luo, X., Yang, L., & Cui, Y. (2021). Continuous monitoring of diabetes with an integrated microneedle biosensing device through 3D printing. *Microsystems & Nanoengineering*, 7(1), 75–75. <https://doi.org/10.1038/s41378-021-00302-w>

- [12] Wilke, Mulcahy, A., Ye, S.-R., & Morrissey, A. (2005). Process optimization and characterization of silicon microneedles fabricated by wet etch technology. *Microelectronics Journal*, 36(7), 650–656.  
<https://doi.org/10.1016/j.mejo.2005.04.044>
- [13] Alicat Scientific, (2022). Thin film deposition techniques. [Thin Film Deposition Techniques | Alicat Scientific](#)
- [14] R. N. Noyce. (1961). Semiconductor device-and-lead-structure.
- [15] V. Sunil, K. Channam. (2017) Synthesis of strongly correlated oxides and investigation of their electrical and optical properties.
- [16] Kim, DE., Sung, IH. (2013). Lithography. In: Wang, Q.J., Chung, YW. (eds) Encyclopedia of Tribology. Springer, Boston, MA. [https://doi.org/10.1007/978-0-387-92897-5\\_1051](https://doi.org/10.1007/978-0-387-92897-5_1051)
- [17] Diez. (2016). The next generation of maskless lithography. EMERGING DIGITAL MICROMIRROR DEVICE BASED SYSTEMS AND APPLICATIONS VIII, 9761, 976102–976102–11. <https://doi.org/10.1117/12.2211052>
- [18] Craigie, C. J. D., Sheehan, T., Johnson, V. N., Burkett, S. L., Moll, A. J., & Knowlton, W. B. (2002). Polymer thickness effects on Bosch etch profiles. *Journal of Vacuum Science & Technology B: Microelectronics and Nanometer Structures Processing, Measurement, and Phenomena*, 20(6), 2229-2232.
- [19] Lin, Y., Yuan, R., Zhang, (2019). Deep Dry Etching of Silicon with Scallop Size Uniformly Larger than 300 nm. *Silicon* 11, 651–658. <https://doi-org.proxy.lib.uwaterloo.ca/10.1007/s12633-018-9948-3>
- [20] Nayak, A.P., Islam, M.S., Logeeswaran, V.J. (2012). Wet Etching. In: Bhushan, B. (eds) Encyclopedia of Nanotechnology. Springer, Dordrecht.  
[https://doi.org/10.1007/978-90-481-9751-4\\_431](https://doi.org/10.1007/978-90-481-9751-4_431)
- [21] Pal, P., Swarnalatha, V., Rao, A. V. N., Pandey, A. K., Tanaka, H., & Sato, K. (2021). High speed silicon wet anisotropic etching for applications in bulk micromachining: a review. *Micro and Nano Systems Letters*, 9(1), 1-59.
- [22] Wind, Jones, H., Little, M. J., & Hines, M. A. (2002). Orientation-Resolved Chemical Kinetics: Using Microfabrication to Unravel the Complicated Chemistry

of KOH/Si Etching. *The Journal of Physical Chemistry. B*, 106(7), 1557–1569.

<https://doi.org/10.1021/jp011361j>

- [23] Zubeľ. (2001). The influence of atomic configuration of ( hkl) planes on adsorption processes associated with anisotropic etching of silicon. *Sensors and Actuators. A. Physical.*, 94(1), 76–86. [https://doi.org/10.1016/S0924-4247\(01\)00690-2](https://doi.org/10.1016/S0924-4247(01)00690-2)
- [24] Zubeľ, & Kramkowska, M. (2004). Etch rates and morphology of silicon ( h k l) surfaces etched in KOH and KOH saturated with isopropanol solutions. *Sensors and Actuators. A. Physical.*, 115(2), 549–556. <https://doi.org/10.1016/j.sna.2003.11.010>
- [25] Wilke, Reed, M. L., & Morrissey, A. (2006). The evolution from convex corner undercut towards microneedle formation: theory and experimental verification. *Journal of Micromechanics and Microengineering*, 16(4), 808–814. <https://doi.org/10.1088/0960-1317/16/4/018>
- [26] Tijanic, Ristic, D., Ivanda, M., Bogdanovic-Rakovic, I., Marcius, M., Ristic, M., Gamulin, O., Music, S., Furic, K., Chiasera, A., Ferrari, M., & Righini, G. C. (2011). Low temperature deposition of SiN<sub>x</sub> thin films by the LPCVD method. *2011 Proceedings of the 34th International Convention MIPRO*, 23–24.